Identification of Methylmercury Export Hotspots in an Industrially-Influenced Great Lakes Coastal Wetland

A THESIS SUBMITTED TO THE FACULTY OF THE UNIVERSITY OF MINNESOTA BY

Amber White

IN PARTIAL FULFILLMENT OF THE REQUIREMENTS FOR THE DEGREE OF

MASTER OF SCIENCE IN WATER RESOURCES SCIENCE

Dr. Nathan Johnson

December 2020

Acknowledgements

I would like to acknowledge all those who helped with the completion of this project. My committee members, Dr. Nathan Johnson, Dr. Sergei Katsev, Dr. Chan Lan Chun, and Dr. Daniel Engstrom for their intellectual support and guidance in the design, data analysis, and writing process. I would also to recognize all those who helped with field sampling and sample analysis, specifically Sam Fink, Jake Daire, Jared Nash, and Dan Fraser from the Johnson lab group, Dr. Jeff Jeremiason and John Pavek from Gustavus Adolphus College, and Marissa Kneer from University of Wisconsin Madison. Sophie Lafond-Hudson played an important role with her never-ending support and guidance as a both a peer and mentor. Finally, I would like to thank my adviser, Dr. Nathan Johnson, for his constant support, encouragement, and constructive feedback that has helped me grow as a scientist and prepared me for the next step in my career.

Abstract

The production and export of methylmercury (MeHg) is a critical first step to accumulation of mercury (Hg) in the lower food web and subsequent accumulation and magnification in game fish. The purpose of this thesis was to identify areas of net MeHg production and export in a freshwater estuary with a history of industrial influence by using ecological boundary delineations. Sediment, porewater and surface water was collected over two seasons from eleven sites encompassing four high-carbon sheltered embayments, two intermediate-carbon clay-influenced bays, and five low-carbon industrially influenced bays in the St. Louis River Estuary (Duluth, Minnesota). Sediment total and methylmercury ranged 3 orders of magnitude with the highest average sediment MeHg and percent MeHg in the isolated, wetland-like sheltered embayments, which had total mercury concentrations similar to non-point source contaminated lakes and wetlands in Northern Minnesota and lower than local industrially influenced bays. Porewater MeHg was highest at sites with higher than average porewater sulfide but low- to middle- range carbon. Sites isolated from the main river channel and without significant tributary inputs experienced surface water MeHg concentrations 3 to 4 times higher than the river, suggesting these areas are net exporters of MeHg to the larger St. Louis River Estuary. Ecologically delineated areas contained characteristically different quantities of Hg and MeHg and appear to be a useful framework for identifying locations likely to experience a net production of MeHg. The results provide a basis for understanding how MeHg can move through freshwater aquatic environments with complex hydrogeochemistry and could form the basis for effective resource management decisions.

Table of Contents:

List of figures

List of tables

Introduction

Methylmercury (MeHg) is a bioaccumulative neurotoxin that accumulates in game fish and can lead to restrictive fish consumption advisories that impair recreational fishing opportunities. MeHg is produced through a microbially mediated process from inorganic mercury, the predominant form of mercury that is directly discharged into surface water, transported atmospherically and precipitated into surface water systems (often far from sources), or has accumulated in sediments as a result of historical industrial activity (Chételat et al. 2018; Lamborg et al. 2002). The methylation process most often occurs in anoxic areas of aquatic environments just below the sediment water interface (Gilmour et al. 1998) by sulfate-reducing bacteria (SRB) (Compeau and Bartha 1985; Benoit et al. 2003) and other anaerobes including iron-reducing bacteria, fermentative Firmicutes, and methanogenic archaea (Parks et al. 2013; Gilmour et al. 2013).

While methylating microbes have been found in a number of environments including freshwater, saltwater, and engineered systems (Podar et al. 2015), wetlands are known to be net produces and exporters of MeHg to their downstream and surrounding environment predominantly because of an abundance of labile carbon, variety of electron acceptors, and relatively long water residence times (St. Louis et al. 1994; Bailey et al. 2017; Hall et al. 2008; Berndt et al. 2012).Wetlands also tend to be heavily vegetated, and the presence of vegetation can increase methylation (Windham-Myers et al. 2009) and slow demethylation (Cesário et al. 2017), both scenarios that can increase net MeHg accumulation in aquatic sediments. Water level fluctuations commonly occur in coastal or seasonal wetlands and can increase methylation because of increased carbon decomposition and continued reduction and re-oxidation of electron acceptors (Eckley et al. 2017; Haynes et al. 2017).

The relationship between mercury methylation and sulfate/sulfide is complex. Because sulfate-reducing bacteria produce MeHg as a byproduct of sulfate reduction, the accumulation of reduced solid phase sulfide (acid volatile sulfide, AVS) is often used as an indicator of historical net sulfate reduction and can be associated with high concentrations of MeHg. While increased aqueous sulfate concentrations have been shown to increase MeHg production (Jeremiason et al. 2006; Myrbo et al. 2017; Gilmour et al. 1992), other studies have demonstrated a reduction in methylation in systems with extremely high porewater sulfide concentrations (300 – 3000 ug L^{-1}) suspected to inhibit MeHg production by reducing the bioavailability of inorganic mercury to methylating bacteria (Benoit et al. 2003; Benoit et al. 1999; Gilmour et al. 1998; Bailey

et al. 2017). The bioavailability of inorganic mercury depends on the presence of other ligands in addition to sulfide, but in anoxic environments dissolved organic carbon (DOC) is the most likely competitor to sulfide for binding mercury. In the presence of both sulfide and DOC, kinetic processes (rather than thermodynamics) may control mercury bioavailability (Hsu-Kim et al. 2013). Additional evidence suggests elevated porewater sulfide may increase MeHg partitioning into porewater from the solid phase, increasing mobility (Bailey et al. 2017) while solid phase carbon may reduce partitioning of both inorganic and methylmercury (Hammerschmidt et al. 2008). Collectively, mercury's interactions with sulfide and carbon can affect both how MeHg is produced and how it partitions between porewater and solid phases (Ullrich et al. 2001).

Production and partitioning of MeHg are two important precursors to the internal loading or flux of MeHg from anoxic sediments into the water column of lakes and rivers where MeHg can easily enter the food web at low low trophic levels (Chen et al. 2009). Internal flux of MeHg can make up a significant portion of MeHg loads in a system, as high as one third of annual loading in a northern Minnesota seepage lake (Hines et al. 2004). In the Delaware River Estuary, water column MeHg has been reported to be 30-70% of porewater MeHg concentrations, suggesting porewater MeHg could be a significant source of water column MeHg (Balcom et al. 2015). Benthic flux studies conducted in the New York- New Jersey Harbor suggest benthic flux of MeHg could be up to 76% of annual MeHg loading to surface waters (Hammerschmidt and Fitzgerald 2008).

Variations in MeHg production and flux can exist on spatial scales of meters to hundreds of kilometers, especially in environments with steep redox gradients, such as in individual peatlands and wetlands. Sediment MeHg concentrations have been found to vary by 2-3x in a single wetland less than 150 meters long as a result of variable sulfate loadings and water level fluctuations (Wasik et al. 2015). This sensitivty to local geochmical conditions can lead to MeHg production hot spots and can be found at the interface of two geochemically and hydrologically distinct areas, such as where wetlands and upland forest soils meet (Mitchell et al. 2008; McClain et al. 2003). These small-scale hotspots can translate to MeHg variations within a downstream water body, seen in Hurley et al. 1995, which demonstrated that watersheds with a high abundance of wetlands and forests can lead to elevated surface water MeHg in areas that do not have point source Hg contamination. These MeHg production and transport hotspots can lead to localized

instances of elevated Hg in fish and wildlife (Drenner et al. 2011; Eagles-Smith and Ackerman 2014). These intra-ecosystem variations make clear the importance of understanding localized mercury cycling patterns in order to make effective management decisions aimed at reducing risk from Hg exposure.

Our study site, the St. Louis River Estuary (SLRE), is a large (50 km^2), shallow, freshwater estuary with elevated fish tissue mercury. The SLRE contains diverse and distinct hydrologic and ecological areas and is heavily utilized for both for both industrial and recreational activities. This spatial heterogeneity has led to the delineation of "habitat zones" which are defined based on differences in geochemical properties and ecological function (SLRA 2002). Imprinted upon this ecological diversity, industrial activity in the Duluth-Superior Harbor has left legacy inorganic mercury contamination while active iron-mining operations near the head of the St Louis River watershed (9283 km^2 drainage area) discharge sulfate, causing surface water concentrations in the main river channel to sometimes exceed 20 mg L^{-1} in the SLRE amidst a background sulfate of < 5 mg L^{-1} (Berndt et al. 2009). Additionally, river flow is partially controlled by hydroelectric dams resulting in anthropogenic water level fluctuations, accentuated by frequent water level fluctuations from Lake Superior's seiche (Sorensen et al. 2004).

Many portions of the upstream St Louis River watershed contain a high percentage of wetlands, which are specifically known to export high concentrations of surface water MeHg and dissolved organic carbon during high flow conditions (Rolfhus et al. 2011). Though MeHg loads from upstream sources are large, previous work (Johnson et al. 2019, in prep) has demonstrated that fish tissue is more elevated in the estuary than the upstream river and downstream Lake Superior. The question of whether elevated fish tissue in the SLRE is due to rapid MeHg production specifically within the estuary or due to ecologically-induced bioaccumulation differences is unclear. A joint Minnesota-Wisconsin Sea Grant funded project is presently seeking to shed light on this question. On necessary part of that evaluation is a thorough understanding of the scope and locations of likely MeHg production areas within the SLRE.

The widely varying geochemical conditions and ecological functions present in the SLRE create situations in which in-situ production and release of MeHg from sediment may be important relative to external sources. The upper estuary has many high-carbon peripheral wetlands and embayments that, combined with instances of prolonged anoxia, harbor redox interfaces that can create potentially high rates of sulfate reduction and mercury methylation. Historical contamination has left inorganic mercury

concentrations elevated in sediment of the lower portions of the SLRE where few riparian wetland habitats exist. Understanding the sources of MeHg to fish in the SLRE is key to evaluating management actions that address consumption advisories in the SLRE.

The main goals of this thesis are to determine if Hg speciation, including sediment MeHg quantitiy and porewater MeHg, varies systematically across ecologically similar habitats and if the geochemical drivers for net production and export of MeHg also vary systematically across these ecologically similar habitats. This was accomplished by dividing our study site into areas with similar ecological characteristics and investigating how the fraction MeHg of THg (indicative of net MeHg production), porewater:sediment concentration ratios (indicative of partitioning into a mobile phase), and surface water:porewater ratios (indicative of the potential for net transport of MeHg away from production zones) vary among these areas. Finally, in order to help discern the potential influence of sediment Hg in industrial areas to overall MeHg loading, concentrations of inorganic mercury in industrially-impacted and natural areas are interpreted in light of the potential for mercury methylation.

Methods:

Site selection: Sites were selected to represent a variety of common, characteristically different ecological habitats in the SLRE. Sheltered bay and clay bay habitat zones are shallow (< 3m) embayments that experience some mixing with the main channel, but are isolated from turbulent, channel mixing mechanisms. Because of their low energy and high primary productivity, they have a high organic carbon content in sediment (averaging 8.6 % and 5.6 % respectively). Industrially influenced bays have lower carbon in sediment (4.7 % excluding one site with greater than 30% carbon from historical logging operations, 8.3 % with this site (Table 1), are generally deeper (5-10 m), and host active or relatively recent industrial activity. They also are also less isolated from the main river channel compared to natural embayments and, due to their proximity to the river mouth, are often exposed to mixing with water from Lake Superior for a portion of the year (Hoffman et al. 2010).

Over two years we visited four sheltered bays, three industrially influenced bays, two clay bays, and mud flats sites (Figure 1, Table S1 in the appendix). Each site was sampled for surface water, porewater, and sediment, typically at three plots to capture variability within an ecological setting. Plots within each

site in the peripheral wetlands of the upstream estuary were chosen in a transect away from shore to target redox gradients that develop because of variations in carbon loading and mixing of embayment water with oxygenated river water (Figure 1). Industrial bays contained little or no vegetation. At other sites, "A" plots are characterized by emergent vegetation and carbon-rich sediment composed mostly of recently deposited, decomposing plant material. "B" plots contain submergent vegetation and more consolidated sediment, while "C" plots contain almost no vegetation and generally have consolidated sediment of a lighter color.

Field methods: Sediment cores were collected using a gravity corer or by directly pushing 7.5 cm diameter polycarbonate core tubes into sediment. At each plot, three replicate cores were extracted and sectioned into acid washed borosilicate glass jars. In 2016, cores were sectioned at 0-2 cm, 2-4 cm, and 4-8 cm intervals with additional replicate cores composited to produce two separate 0-4 cm samples (data in appendix Table S5). In 2017 triplicate cores were only sectioned into 0-4 cm composites. Jars were filled to the top with saturated sediment, sealed with electrical tape, stored in a cooler on ice during transfer to an anaerobic chamber (98 % N_2, 2 % H_2) in the lab within 6 hours of collection. These composite samples were used for solid phase and porewater analyses. Surface water was collected using clean hands methods from each plot using double-bagged mercury-free PETG bottles for filtered (0.45 µm polyethersulfone, Environmental Express) total- and methyl- mercury measurements. Samples were also preserved with 0.5% by volume trace metal grade concentrated HCl and stored double bagged in the dark. Field measurements of temperature, conductivity, and dissolved oxygen (DO) were made using a Hydrolab multiparameter Sonde calibrated daily.

Porewater was extracted from sediment composites following homogenization using 0.2 µm Rhizons (tension lysimeters) (Seeberg-elverfeldt et al. 2005) connected to stainless-steel needles inserted into acid washed, oxygen free, gas tight, evacuated serum bottles. After 8 – 24 hours of filtering in an anaerobic environment, filtered porewater samples were allocated and preserved for total- and methyl- mercury (0.5 % trace metal HCl), DOC (0.2 % phosphoric acid), and sulfate (stored cold). Porewater sulfide was collected in a separate oxygen free serum bottle preloaded with 0.2% Zinc Acetate and 0.2% 6M Sodium Hydroxide. Methylation potential measurements with enriched stable isotopes were performed but did not figure prominently into the present analysis. Methods and results are provided in the appendix. Lab incubations to

quantify flux from sediment to surface water were also performed as outlined in the appendix, but are not used in the present interpretation.

Analytical methods: Total sediment organic carbon is measured using a Thermo Scientific FLASH EA™ 1112 Elemental Analyzer; dissolved organic carbon (DOC) is measured using a Shimadzo TOC analyzer; acid volatile sulfide (AVS) and the simultaneously extracted metals (specifically iron) is measured through 1 M HCl extraction in sealed glass diffusion chambers with a colorimetric analysis for sulfide and weakly extractable ferrous iron. This weakly extractable ferrous iron was quantified on HACH DR5000 UV-VIS using phenanthroline (Eaton et al. 2005; LaFond-Hudson et al. 2018). Sulfate is analyzed using a Dionex ICS 1100 system. Total and methylmercury was analyzed through acid digestion and isotope-dilution mass spectroscopy as outlined in (Johnson et al. 2016). Total mercury is measured by a stannous chloride reduction using a Brooks Rand MERX Model III Atomic fluorescence spectrophotometer. MeHg is measured using an isotope dilution method. Before distilling the sample, $Me^{199}Hg^{+}$ is added to the sample under Argon gas to quantify recovery. The sample is then ethylated to create volatile methylethylmercury, separated on a GC column, and quantified following pyrolysis on an Agilent 7700 ICP-MS connected to a Brooks Rand MERX analyzer (Bloom 1989; Hintelmann et al, 1997; Jackson et al. 2009).

Net MeHg transport analysis methods: Two ratios were used to describe the potential for MeHg flux among ecosystems in the SLRE (see Figure 2). The first ratio was used to contextualize the role of isolation from the main river channel in creating conditions sensitive to a buildup of internally-loaded MeHg in the overlying water. This is the ratio of surface water MeHg at each plot (A, B, and C) to surface water MeHg in the adjacent main river channel and is expected to be proportional to MeHg transport induced by mixing from cyclical water level fluctuations that exchange water between the main river channel and embayments. A ratio greater than one means surface water MeHg is higher in the embayment location compared to the main river. Since the main river channel has a short residence time and would be carrying upstream MeHg loads (from the rest of the watershed), elevated surface water MeHg in embayments suggests the presence of some other local source of MeHg to the water column. A second ratio of porewater MeHg (0-4 cm) to embayment surface water was used as a net indicator of the sustained gradient available to drive diffusive

transport from sediment to overlying water. A ratio close to or higher than one means the forces that remove MeHg from the surface water, such as mixing or demethylation, are happening quickly enough to support a gradient to drive MeHg transport from sediments into the surface water. A ratio close to or below 1 means that MeHg may be produced in surface water, or that little transport is occurring to move MeHg away from the location of production in sediment.

Statistical Methods: Measurements were made in triplicate sediment and porewater samples from each plot and presented as individual independent measurements. 2016 data is for the top 0-2 cm section and 2017 data is for the top 0-4 cm section. All samples were used when making comparison among sites visited in both years because average sediment MeHg did not vary significantly between 2016 and 2017 at each site (SI Figure S12). All variables were assessed for normality using histograms and Q-Q plots. All data was log transformed prior to statistical analysis for normality. One-way Analysis of Variance (ANOVA) was used to determine significance between habitat zones at $\alpha = 0.05$. Regressions are based on simple linear regressions and assessed for significance using F-tests.

Results and discussion

Bulk Elemental Sediment Geochemistry

Inorganic Hg: Inorganic Hg concentrations in sediment were largely below 200 ng g^{-1} dw (75% of sites below 195 ng g^{-1}) (Table 1), which is consistent with observations in northern Minnesota's pristine Voyagers National Park (Wiener et al. 2006), atmospherically dominated Spring Lake in northeastern Minnesota (Hines et al. 2004), other parts of the St. Louis River watershed (Bailey et al. 2017), and the Florida Everglades (Gilmour et al. 1998). Mean sediment inorganic mercury was significantly different ($p < 0.01$) between sheltered bays (154 ng g^{-1} dw) and clay bays (59 ng g^{-1} dw) and clay bays and industrial bays ($p = 0.01$, average 243 ng g^{-1} dw). Notably, mean inorganic Hg is not significantly different between industrial bay and sheltered bay; however, the variance in inorganic Hg in the industrial bays was large, ranging from 4 ng g^{-1} dw to 1822 ng g^{-1} dw. While the average IHg for the industrial bays (243 ng g^{-1}) is only slightly elevated relative to locations unimpacted by industrial inputs, two specific sites, IB1 and LEF, have lower average inorganic Hg (51 and 11 ng g^{-1} respectively) compared to the rest of the habitat zone

(average 625 ng g $^{-1}$). Cores from IB1 and LEF contained coarse material, had higher solids contents (65-80%) and lower carbon (0.4%-7%) than most other sediment in the SLRE. Additionally, LEF sediment inorganic Hg decreased from 169 ng g $^{-1}$ dw in 2016 to 11 ng g $^{-1}$ dw in 2017. We suspect that these two sites may have been influenced by dredging activities that are common in the lower estuary and contribute to significant variance in inorganic Hg concentrations of the industrial bay zone.

In sediments from aquatic environments dominated by disperse atmospheric inputs of Hg, sediment inorganic Hg concentrations correlate strongly with sediment carbon, due to the strong association of Hg with carbon in the solid phase during transport to the sediment. This relationship (Figure 3B) is significant in sheltered bays (R^2 = 0.85, p = <0.001) and clay bays (R^2 = 0.34, p = 0.04) but not industrial bays (R^2 = 0.035, p = 0.32). Some of the highest inorganic mercury concentrations are found in portions of the industrial bay habitat zones with very low carbon (circled areas of Figure 3A and 3B). Inorganic Hg concentrations at most sites in the upper portion of the estuary (CB and SB) are similar to other non-industrially impacted northern Minnesota locations and have a significant relationship between sediment carbon and inorganic Hg. While the source of Hg cannot be unambiguously identified from total mercury or even carbon-normalized total mercury, most ecosystems in the upper river do not have total mercury quantities that suggest significant point source contamination. Isotopic methods for distinguishing Hg from different sources are a potential method for understanding the source of mercury (Lepak et al. 2015) and Hg isotope data in the SLRE should be available soon. Differences in carbon-normalized inorganic Hg suggest the presence of occasional historical point source contamination within the industrial bay habitat zone.

Methylmercury: Sediment MeHg concentrations averaged 1 ng g^{-1} dw in the entire dataset, ranging from 0.03 – 6.42 ng g^{-1} dw (Table 1). Sediment MeHg was, on average, significantly higher in the sheltered bays than in the clay bays (p= 0.03) and industrial bays (p < 0.001) but similar between clay bays and industrial bays (p = 0.58). This suggests that, regardless of Hg origin or carbon quantity, at long time scales when the processes controlling Hg cycling in the SLRE sediment are at equilibrium, sheltered bay sediment on average contains more MeHg on the solid phase compared to industrial bays and clay bays.

One shallow, heavily vegetated sheltered bay, Perch Lake (SB2), stood out from the rest of the sheltered bays for having distinctively lower solid-phase MeHg concentrations in sediment. SB2 is a small sheltered bay, isolated from the main river channel by a culvert that limits the amount of mixing that occurs

between the embayment and the river channel. SB2 has a lower sediment MeHg (Table 1) (0.67 ng g^{-1} dw) and percent MeHg (0.6%) than all other sheltered bays (1.67 ng g^{-1} dw and 1.8% respectively). We suspect this difference is a result of a restricted bay-river exchange area and a build-up of anoxic conditions in the overlying water (DO saturation just below water-air interface of 17%, 57%, and 102% for A, B, and C plots respectively, appendix Table S4) that appears to have led to more rapid AVS accumulation compared to other sheltered bays (31.8 umol g^{-1} vs 10.2 umol g^{-1} respectively). High levels of sulfide can inhibit the production of MeHg by reducing the amount of inorganic mercury available for methylation(J. M. J. Benoit et al. 2003; C. Gilmour et al. 2018). Because SB2 is different from other sheltered bays included in this study and not characteristic of many other locations in the SLRE, it is listed individually in tables and charts and has been excluded from the following ANOVA among habitat zones and treated separately in regressions unless otherwise stated.

Carbon and acid volatile sulfide (AVS): Sediment carbon is significantly higher in the sheltered bay than the industrial bay ($p = 0.04$) although there is no difference between sheltered bay and clay bay habitat types. Because MeHg production is a microbially mediated process, the accumulation of reduced sulfur on the solid phase (AVS) is often used as an indicator of activity of sulfate-reducing bacteria, recognized prevalent Hg methylators. AVS is significantly higher in the sheltered bays than industrial bay ($p < 0.001$) and clay bay ($p < 0.001$). This suggests that the riparian wetlands are more conducive to MeHg production than the industrial bays, based on carbon and AVS and trends observed in the estuary.

Methylmercury production among habitat zones

Since bulk elemental quantities and speciation, reflective of long-term geochemical processes differed significantly among habitat zones, further investigation of the patterns in MeHg production among habitat zones and geochemical drivers across ecosystems will help determine if the sediment of certain habitat zones are a source of MeHg to the water column. To investigate differences in MeHg production across habitat zones, MeHg production was quantified and placed in the context of variations in inorganic Hg concentrations, carbon, or AVS. Because sediment MeHg concentrations are the result of net methylation, demethylation, and sediment inorganic Hg, sediment % MeHg (percent of total mercury present as methylmercury), is often used as a metric for "methylation efficiency" to better understand *in-situ* MeHg

production. Overall, sediment % MeHg in the SLRE varied by 2 to 3 orders of magnitude (Table 1) and contained significant variance within habitat zones. This reflects a wide range in the ability of local conditions to transform inorganic Hg into MeHg. On average, % MeHg in the SLRE is similar to lake sediments in other aquatic environments including the upstream SLRE watershed (Bailey et al. 2017), the agriculturally-impacted Florida Everglades brackish wetlands (Gilmour et al. 1998), and the coastal San Francisco Bay Delta (Heim et al. 2007). Average % MeHg in sediment is much lower, however, than in wetlands with elevated surface water sulfate concentrations of the St. Louis River watershed (Johnson et al. 2016) and boreal freshwater wetlands in Sweden (Tjerngren et al. 2012). The sheltered bays (1.8%) and clay bays (2.0%) have, on average, similar % MeHg ($p = 0.46$) and both have significantly higher % MeHg than the industrial bays (1.0%, $p < 0.01$ for both clay bays and sheltered bays), which suggests both the sheltered bays and clay bays produce more MeHg on a relative per-gram inorganic Hg basis. The highest % MeHg was observed at sites with low carbon normalized inorganic Hg (Figure 3A) (i.e. more carbon per inorganic Hg present) while most of the sites with high inorganic Hg have little carbon (likely due to point source contamination) and produce low % MeHg. However, some industrial bay sites with low inorganic Hg:Carbon ratios have % MeHg similar to sheltered and clay bays (squared in points of Figure 3A). This suggests that some locations with elevated inorganic Hg in sediment may be efficient at producing MeHg if sufficient carbon is present to drive microbial methylation. Given an influx of carbon, these high Hg sites could see an increase in absolute MeHg production, if inorganic Hg remains high in methylating zones near the sediment surface.

The accumulation of reduced sulfur on the solid phase (AVS) is often used as an indicator of activity of sulfate-reducing bacteria, recognized contributors to Hg methylation in many ecosystems. The highest observed % MeHg in the SLRE occurs between AVS values of 1 and 10 μmol g^{-1} (Figure 4a). Below and above this range % MeHg is lower. However, because AVS increases with carbon (Figure 4b), differentiating the effects of elevated carbon versus elevated AVS on methylation is difficult. Peak % MeHg is in sediment with 4-7 % carbon (Figure 4c) but peak AVS is in sediment with 9-15 % carbon. Even though AVS remains relatively high after 15 %, % MeHg stays low. A potential interpretation of these patterns is that peak methylation occurs in a middle range of carbon and AVS where enough carbon is present to support microbial

activity yet not too much carbon or sulfide, both of which could reduce methylation due to bioavailability of inorganic Hg in high carbon and high sulfide environments (Hammerschmidt et al. 2008).

Most of our sites have relatively low ratios of AVS to HCl-extractable iron (Figure 5). While we do not have porewater iron measurements, we do not expect all porewater iron to be completely bound to porewater sulfide given porewater sulfide concentrations are largely below 10 uM. When ferrous iron in sediment is mostly complexed with sulfide, additional sulfur loading can cause dissolved sulfide to accumulate in porewaters (Mehrotra et al. 2005; Bailey et al. 2017; Schartup et al. 2014; Johnson et al. 2019). Our sites had ratios of AVS:HCl-extractable iron well below 0.1 (below 10% ferrous iron complexed with AVS), indicative of a stoichiometric excess of iron relative to sulfur in the sediment. Though variability existed in the overall relationship between porewater sulfide and AVS:HCl-extractable iron, the relationship was significant within each habitat zone, suggesting that the stoichiometry of Fe and S in sediment could impact the presence of dissolved sulfide in porewater and therefore the rates of Hg methylation. Interestingly, while some sediment from SB2 had the highest AVS:Fe ratio, these samples do not have the most filter-passing sulfide. Filter-passing sulfide likely comprises the species that complexes with Hg to reduce uptake by bacteria, though detailed interactions among DOC, dissolved sulfide, and inorganic Hg are complex (Hsu-Kim et al. 2013) and beyond the scope of our study. The low quantity of MeHg produced in SB2 could potentially be due to reduced partitioning of inorganic Hg into porewaters, rather than reduced availability of dissolved inorganic Hg, caused by the combination of both high solid phase sulfide (Hammerschmidt and Fitzgerald 2004) and high organic matter (Hammerschmidt et al. 2008).

Partitioning of MeHg into porewater

Partitioning of MeHg from the sediment into porewater is an important step to increasing the mobility of MeHg from areas of net production. Average porewater MeHg concentrations (Table 2) were significantly different between all three zones ($p < 0.01$ for all) and were highest in clay bays despite sediment MeHg and %MeHg being highest in sheltered bays. However, even though sheltered bays have a higher average porewater MeHg, sediment MeHg, and higher sediment %MeHg than industrial bays, the bulk sediment MeHg concentrations alone does not explain porewater MeHg concentrations (Figure 7). The relationship between sediment and porewater MeHg is only significant in clay bays and nearly significant in the industrial

bays. The lack of a consistently significant relationship between sediment and porewater MeHg suggests that the production of MeHg and accumulation on the solid phase may not be the limiting step in defining MeHg quantity in porewater and that other factors could be controlling the partitioning into porewater.

The average effective partitioning coefficient for MeHg, log K_d, is the ratio of porewater MeHg to sediment MeHg. On average, log K_d was significantly lower in clay bays than sheltered bays and industrial bays ($p < 0.001$ for both), which means more MeHg is present in the porewater per solid phase MeHg in clay bay sediment than in any other zone. Average K_d for MeHg was not significantly different between sheltered bay and industrial bay, despite sheltered bays having significantly more MeHg in the porewater. These disconnects between solid phase MeHg and porewater MeHg partitioning could be caused by variations in solid phase carbon and porewater sulfide.

Porewater sulfide is significantly higher in sheltered bays ($p < 0.01$) and clay bays ($p < 0.001$) compared to industrial bays, most likely because of higher carbon and greater sulfate-reducing bacteria activity (demonstrated by elevated AVS). Porewater sulfide is negatively correlated ($p = 0.006$, $R^2 = 0.25$, Figure 8a) to log K_d in clay bays, consistent with the interpretation that additional porewater sulfide may pull more MeHg into the porewater. However, in the sheltered bays, porewater sulfide is positively correlated with log K_d (Figure 7, $p = 0.02$, $R^2 = 0.18$). Solid phase carbon can influence partitioning of MeHg into porewater (Hammerschmidt et al. 2008). This is confirmed by our data and a significant and fairly-strong linear regression between log K_d and solid phase carbon in the sheltered bays ($p < 0.001$, $R^2 = 0.46$). There is no significant relationship between porewater sulfide and log K_d in the industrial bays. These results are consistent with other studies that demonstrated decreases partitioning to porewaters in environments with higher organic carbon on the solid phase (Hammerschmidt et al. 2004; Hammerschmidt et al. 2008) while sulfide increases partitioning to porewater (Bailey et al. 2017). Mercury binds to different functional groups on organic carbon (Aiken et al. 2011; Manceau et al. 2015; Nicolas S. Bloom et al. 2003) and a while thorough analysis of the carbon involved in binding Hg was beyond the scope of this study, evidence suggests reduced thiol groups are often involved (Gerbig et al. 2011; Hesterberg et al. 2001; Poulin et al. 2017; Bower et al. 2008). Though porewater DOC varies only by a factor of two across the dataset, there is no significant trend in any habitat zone between log K_d and porewater dissolved organic carbon, which also does not vary significantly by habitat zone (Figure 8c). This suggests that variations in MeHg partitioning in the SLRE

sediment are not impacted by porewater dissolved organic carbon quantity, but is strongly affected by solid phase carbon and porewater sulfide. In contrast, DOC is influential in transporting MeHg in upstream surface waters of the St. Louis River (Berndt et al. 2012).

To contextualize the role of isolation from the main channel in creating conditions conducive to a buildup of internally-loaded MeHg in the overlying water, we calculated a ratio of surface water MeHg at each plot (A, B, and C) to surface water MeHg in the main river channel (see Figures 1 and 2 in methods). A ratio greater than 1 means surface water MeHg is higher in the embayment compared to the main river. The highest ratios were found in the clay bays and sheltered bays (Figure 9), with embayment:channel ratios of greater than 2 found at predominantly A plots with low dissolved oxygen. With only one exception, industrial bays had high dissolved oxygen waters with embayment:channel ratios between 1 and 1.5. The two highest embayment:channel ratios at industrial bays were from A plots, which suggests the A plots (near-shore, shallow and more vegetated) in the industrial bays may, on occasion, transport MeHg or experience transport processes similarly to other A plots in the sheltered bay and clay bay zones.

The highest bay to channel ratios were found at A plots with low dissolved oxygen while B and C plots tended to stay almost completely oxygenated (dissolved oxygen greater than 80%) but still consistently contained ratios greater than 1 (up to 1.5). The consistently elevated ratios in the sheltered and clay bays suggests that, in response to diffusive exchange between embayment locations and the main channel, the sheltered and clay embayments can be net exporters of MeHg to the larger SLRE system. This is important because MeHg often enters the food web through surface water (Chen et al. 2009; Wiener et al. 2006).

While the embayment:channel ratio is useful for identifying areas of surface water MeHg sources to the larger estuary, the ratio is sensitive to upstream loading which varies seasonally and with river flow (appendix Figure S13). 2016 sampling timeframe occurred following a high precipitation rain event that raised river flow from 3500 cfs to 7200 cfs while 2017 sampling saw flows drop from 2000 cfs to below 500 cfs. As a result, surface water MeHg in the main channel was elevated in 2016 (average 0.21 ng L^{-1}: 0.14, 0.22, 0.26 at our three sampling points) compared to 2017 (average 0.13 ng L^{-1}, 0.15, 0.16, 0.09). This helps to explain why 2016 ratios are, in general, lower than 2017. While river flows and temporal variations in surface water MeHg concentrations are important for contextualizing the embayment:channel ratio, a full analysis of surface water measurements is beyond the scope of this thesis. Regardless, the elevated MeHg in

embayments relative to channel unambiguously identifies embayments as a potential contributor to internal MeHg loading to the larger estuary system.

Even though the elevated bay to channel ratios suggest internal sources of MeHg to SLRE surface waters, the nature of sources within the embayment cannot be determined solely by considering the bay:channel interface. If MeHg is produced primarily in anoxic sediments and transported to surface water, surface water MeHg concentrations are the net result of mixing, demethylation, adsorption, and biological uptake. In light of this, the ratio of porewater MeHg to surface water MeHg can be used as a net indicator of a sustained gradient with the potential to drive diffusive transport from sediment to overlying water (figure 2). A ratio close to or less than 1 means the processes that remove MeHg from the local surface water, such as mixing or demethylation, aren't happening quickly enough to support a gradient to drive diffusive MeHg transport from sediments into the surface water. In anoxic waters, a ratio near to or less than one could also be a result of MeHg production in surface waters. Conversely, a ratio greater than 1 suggests that mixing or demethylation mechanisms in the surface water could maintain a diffusive flux gradient by keeping surface water MeHg lower relative to MeHg in porewater, potentially driving diffusive flux into the overlying surface water.

Most sites had porewater:surface water ratios close to or greater than one (Figure 10, line drawn at porewater:surface water ratio =1) which means most of our sites have a concentration gradient capable of supporting diffusive flux from sediments to surface waters. Three near-shore sites with emergent vegetation (CB1A, SB2A, SB3A) had porewater:surface water ratios less than one during 2017. All three of these sites had low (less than 30% saturated) dissolved oxygen and bay to channel ratios of 2.5 - 4.5. Since porewater MeHg was less than surface water MeHg at these sites, they may experience water column methylation, especially since low dissolved oxygen suggests minimal mixing with channel surface water. Most of the remaining sites, however, have both elevated bay to channel ratios (Figure 9, ratio of 1 at black line) as well as elevated porewater:surface water ratios. This suggests that the elevated MeHg in embayment surface waters (relative to the channel) lies in the middle of an overall gradient supportive of diffusive/dispersive flux from zones of net methylation in the embayment sediment through the embayment surface water and to the river channel.

Implications for net MeHg flux from embayments in the SLRE

In freshwater aquatic systems, carbon plays an important role in both carrying inorganic Hg to sediment and driving the biological production of MeHg, so higher C in sediment is often accompanied by higher MeHg. However, the complex history of industrial activities in the SLRE make the relationship between C, iHg, and MeHg less clear. Sediment IHg concentrations varied significantly throughout the estuary but sediment MeHg did not covary strictly with the quantity of sediment inorganic Hg due to wide ranges of methylation efficiency (Figure 6). Despite elevated inorganic Hg concentrations in the industrial bays, sheltered bays and clay bays had similar or higher absolute quantities of MeHg and the highest average sediment MeHg concentrations were found in the sheltered bay habitat type.

Sheltered bays and clay bays were consistently higher than industrial bays in terms of carbon and AVS, important indicators of the biogeochemical drivers of MeHg cycling. While most of the industrial bays had low carbon, some high carbon plots within the industrial bays suggests an influx carbon could mobilize potential legacy Hg contamination to the more bioavailable MeHg pool. Patterns in the data reveal that large inorganic Hg in conjunction with enough organic carbon and a moderate rate of sulfate reduction (as indicated by AVS accumulation and low Fe:AVS ratios) produced the highest MeHg concentrations in sediment of the SLRE. Habitat zones that experience moderate rates of sulfide accumulation (1-10 μmol g-1 AVS) and have moderate carbon (up to 5-10%) appear to be most efficient at producing MeHg per gram of inorganic Hg present. Habitat zones with high AVS (greater than 20 μg g-1) appear to experience sulfide inhibition, which could limit MeHg production by reducing the amount of inorganic Hg available for methylation. High carbon was associated with higher AVS and sediment % MeHg until a point (~10 μmol g-1 dw) after which % MeHg was consistently low. Most of our sites were below this cutoff, suggesting a capacity for increased methylation in the SLRE especially in the industrial bays.

Porewater MeHg was not consistently related to either sediment MeHg or % MeHg in the habitat zones. Partitioning to porewater was decreased by high solid phase carbon and increased with elevated porewater sulfide. This suggests that additional porewater sulfide at presently low porewater sulfide sites could increase partitioning of MeHg in the surface waters of the SLRE. Surface water MeHg was higher at A plots in the sheltered bays, clay bays, and industrial bays than the main channel, especially in sheltered and clay bays at locations and times with low dissolved oxygen. The low DO in surface water may enable

more rapid transport from sediment, slow demethylation in surface water, or enable water column methylation to occur. The prevailing trend of decreasing MeHg concentration from porewater to embayment surface water to channel surface water provides strong evidence that bays and anoxic sediment in near-shore areas are potential sources of MeHg to the larger estuary system. Quantifying the magnitude of this source relative to upstream sources will require constraining the magnitude of exchange among each of these pools of MeHg.

The significant differences found between habitat zones with respect to small scale mechanistic processes, such as % MeHg and log Kd, create a sediment "mercury fingerprint" for the SLRE (Table 3), resulting in observable differences at a larger scale when comparing surface water MeHg in embayments to main river channel water. The ANOVA comparison of solid phase mercury trends suggests that at long time scales (which control the accumulation of MeHg on the solid phase) MeHg production is significantly different between each of the habitat types. This result supports the aggregation of SLRE sediments by habitat type in evaluating the net production of MeHg in sediment and partitioning porewaters. Because of this, we recommend habitat type should be considered when evaluating remediation or restoration efforts in the SLRE based on the conversion of sites from one dominant ecosystem type to another, which has implications for Hg cycling in the SLRE.

Conclusion

In the diverse ecological settings of the SLRE, the greatest potential for MeHg production, as indicated by % MeHg in sediments, occurs in embayment settings which are isolated from the main river-channel flow, anoxic, heavily vegetated, and enriched with carbon and sulfur (Sheltered and Clay Bays). This is consistent with previous studies demonstrating the importance of sulfate-reducing and other anaerobic bacteria in producing methylmercury (Compeau and Bartha 1985; Parks et al. 2013b; Bravo et al. 2018; Brown et al. 2011). In many cases, sediment from embyaments with less isolation from the main channel that contain less anoxia, vegetation, and carbon (Industrial Bays) have higher THg, but this does not consistently translate to greater quantities of MeHg in sediment, likely due to the lack of fuel for anaerobic microbial activity.

The potential for MeHg mobilization from anoxic sediments, as indicated by greater relative quantities of MeHg in sediment porewater (low K_D), differed between the two types of heavily vegetated embayments. Clay bays had less carbon in sediment, but consistently higher dissolved sulfide and a higher quantity of MeHg in porewater, which is supported by previous studies (Kneer et al. 2020; Bailey et al. 2017; C. Gilmour et al. 2018). We specifically observed log K_d for MeHg decreasing in concert with increasing porewater sulfide in the clay bays. However, at similar sulfide levels in the higher carbon sheltered bay sediment, porewater partitioning was lower, possibly because of the nature of MeHg associations with solid phase carbon.

Across the habitat types included in this study, the production of MeHg in sediment and partitioning of MeHg to porewaters and surface waters were consistently related to underlying biogeochemical processes, especially carbon and sulfur cycling in sediment. It is noteworthy that the net effect of these processes appear to result in delineations of MeHg cycling that are consistent within habitat type delineation. A full description of the specific mechanisms defining these interactions would require more investigation; however, our study shows that areas with similar ecological habitats can be aggregated to describe Hg speciation and the potential for export of MeHg in complex freshwater environments. Specifically, freshwater sediments in heavily-vegetated nearshore areas can be a sustained source of MeHg to a local connected waterbody and should be one consideration when addressing restoration or remediation of sediments in aquatic systems prone to mercury contamination.

While MeHg quantity in the sediment and porewater was explained well by the habitat type, MeHg in the surface water was not always uniform within ecologically similar habitats and appears to be more sensitive to internal spatial variations within a site and proximity to main river channel. We recommend a more spatially discrete analysis of surface water trends and transport processes in future work. Based on our study, sediment mercury and methylmercury patterns can be effectively described and aggregated using ecological characterization in ecosystems with variable habitat types, such estuaries, deltas, anthropogenically influenced waters, and reservoirs.

Our finding that a simple delineation across habitat type rather than a full geochemical description of the underlying processes could allow for a modeling framework that supports the strategic assessment, remediation, and restoration of spatially complex contaminated freshwater environments. Potential

applications include developing remediation strategies that focus clean-up activities on specific habitat types prone to MeHg production or engineering changes that prevent the geochemical conditions that support methylation, for example by increasing oxygenation of anoxic sites. Our work might also be applied in systems facing similar contamination challenges beyond Hg given the importance of geochemical parameters like carbon concentration and redox processes to the transport of other contaminants of concern (Hsu et al. 2016; Landrum and Faust 1994; Petosa et al. 2010; Alimi et al. 2018).

Much of the spatial variation in observed sediment and porewater mercury speciation are consistent with variations in habitat type, which is based on widely understood and easy to define ecological characteristics. We specifically used previously described habitat types in the SLRE that aggregated area based on sediment composition, vegetation type and abundance, and anthropogenic influence. We believe these novel results support a framework that can inform management, remediation, and restoration of spatially complex contaminated freshwater environments.

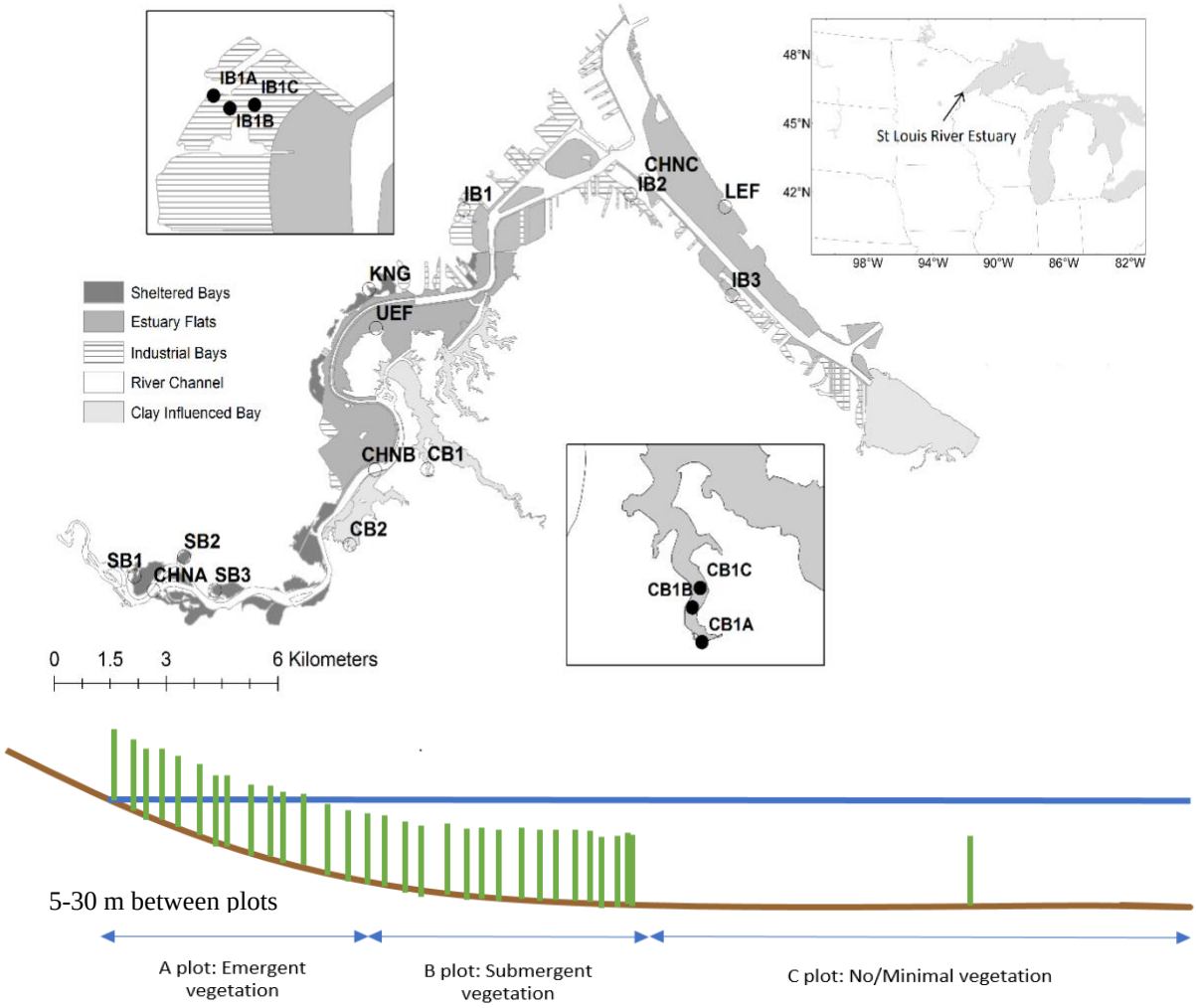

Figure 1: Map of St. Louis River Estuary (SLRE) and sites visited. See appendix Table S1 for more site description. Inset demonstrates near shore to offshore plots: "A" plots are closest to shore and have predominantly emergent vegetation, "B" plots are slightly off shore and have submergent vegetation, and "C" plots are furthest from shore and have little to no vegetation. This sampling scheme was maintained for the 2016 and 2017 sampling seasons.

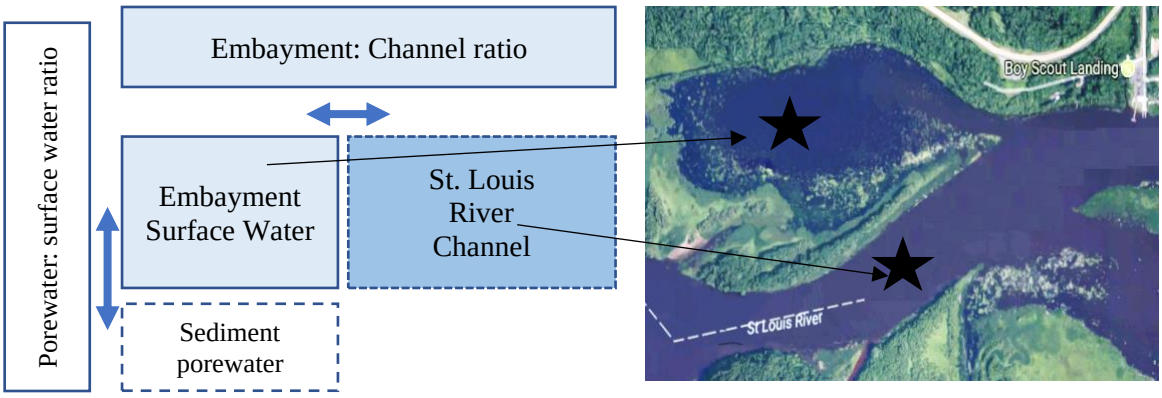

Figure 2: Conceptual diagram describing ratios devised to describe flux and transport in the SLRE.

Embayment to channel ratios ($\frac{Embayment\ surface\ water\ [MeHg]}{Channel\ surface\ water\ [MeHg]}$) were calculated using surface water MeHg in a specific embayment and then compared to the channel surface water MeHg. This ratio allowed us to contextualize the MeHg in an embayment in terms of the upstream MeHg loads using the channel MeHg concentrations. Porewater to surface water ratio ($\frac{Porewater\ [MeHg]}{Surface\ water\ [MeHg]}$) is a ratio of porewater MeHg and surface water MeHg and used to determine if a gradient for net observable MeHg flux from porewater into overlying surface water is present.

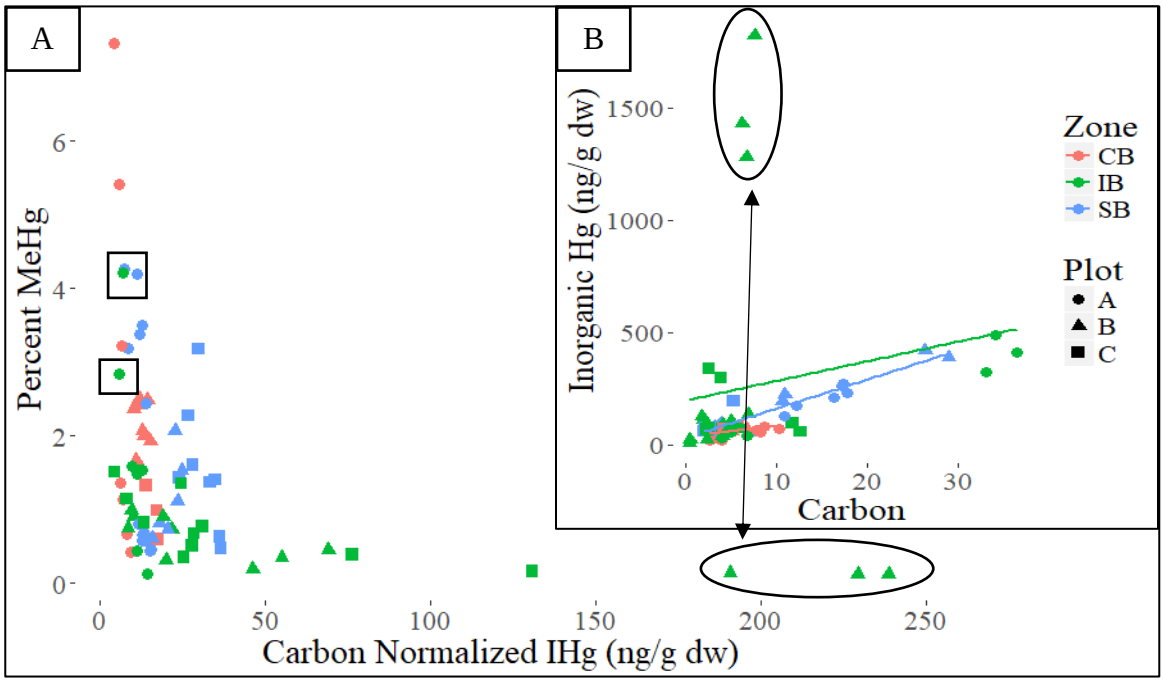

Figure 3: Sediment percent MeHg versus carbon normalized inorganic Hg concentrations (A) and inorganic Hg versus organic carbon (B). Plot is represented by shape: circles (A- emergent vegetation), triangles (B- submergent vegetation), and squares (C- no vegetation). Habitat zone is represented by color: red (clay bays), green (industrial bays), blue (sheltered bays). Samples were collected in July 2016 or 2017 from the top 0-2 and 0-4 cm of sediment respectively. Lower inorganic Hg:Carbon ratios mean more carbon present per ng of inorganic Hg and are indicative of atmospherically dominated systems, or systems where the main source of Hg is not from industrial releases, where inorganic Hg associates strongly with solid phase organic carbon. The circled points represent potentially point source contaminated areas of the industrial bays while the squared points represent areas of the industrial bays that have higher percent MeHg potentially because of higher carbon than other parts of the industrial bays.

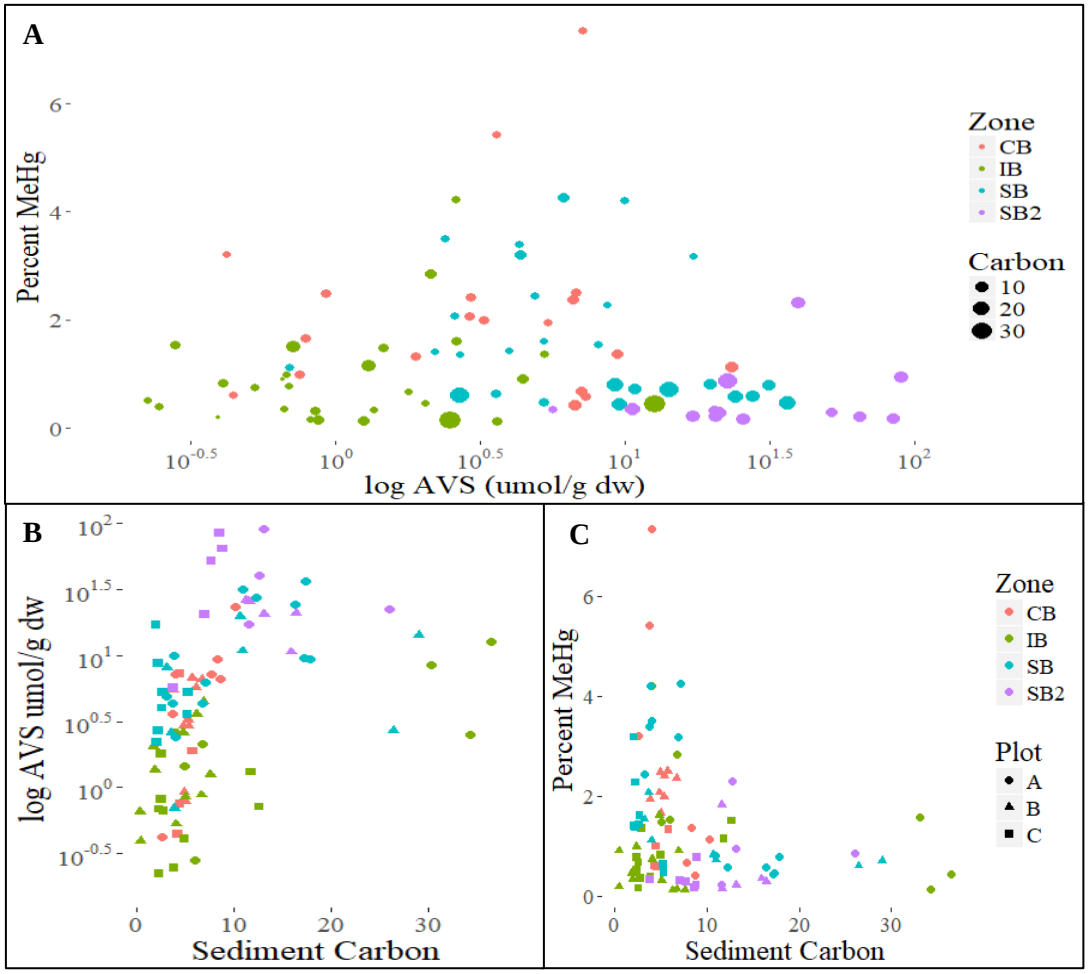

Figure 4: a) AVS plotted versus carbon; b) sediment %MeHg versus carbon; c) sediment %MeHg versus AVS, which is used as an indicator of SRB activity, the known principle methylators in freshwater systems. Dot size indicates carbon content and color indicates habitat zone. For these graphs, SB2 is included to evidence of suspected sulfide inhibition in that embayment.

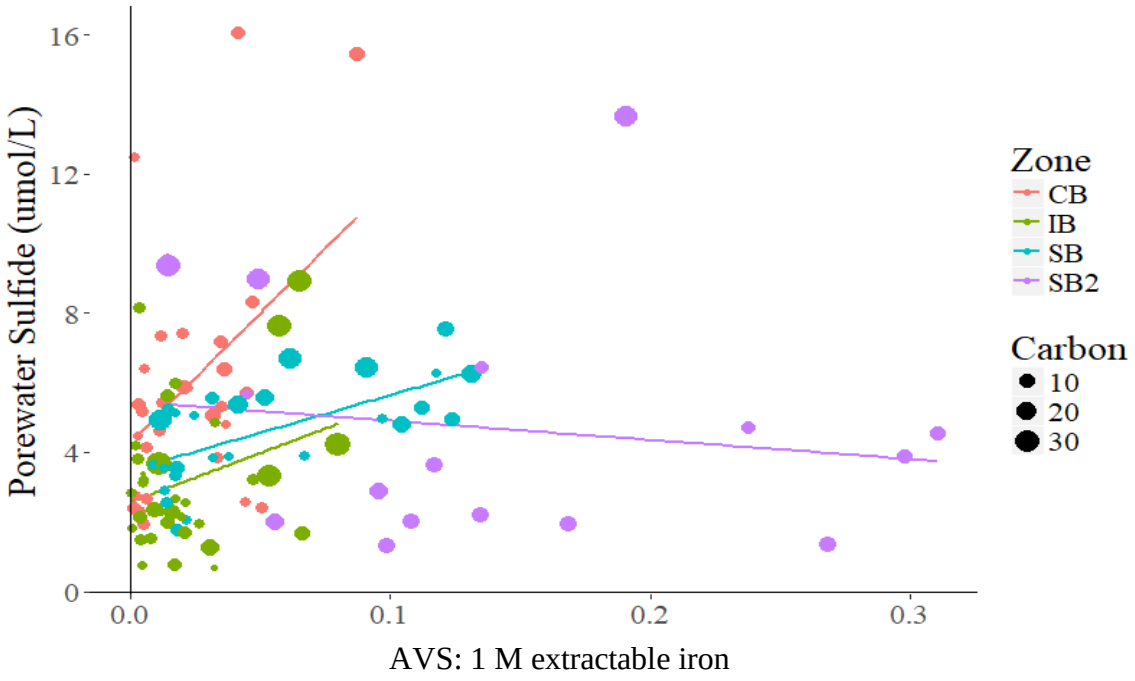

Figure 5: Molar ratio of solid phase sulfide to 1 M extractable iron. Points are colored according to habitat zone, with SB2 colored separately from the other sheltered bays, and sized according to sediment organic carbon. Dots are colored according to habitat zone but list SB2 as an individual site separate from the rest of the sheltered bays. Bubble size indicates carbon content in percent

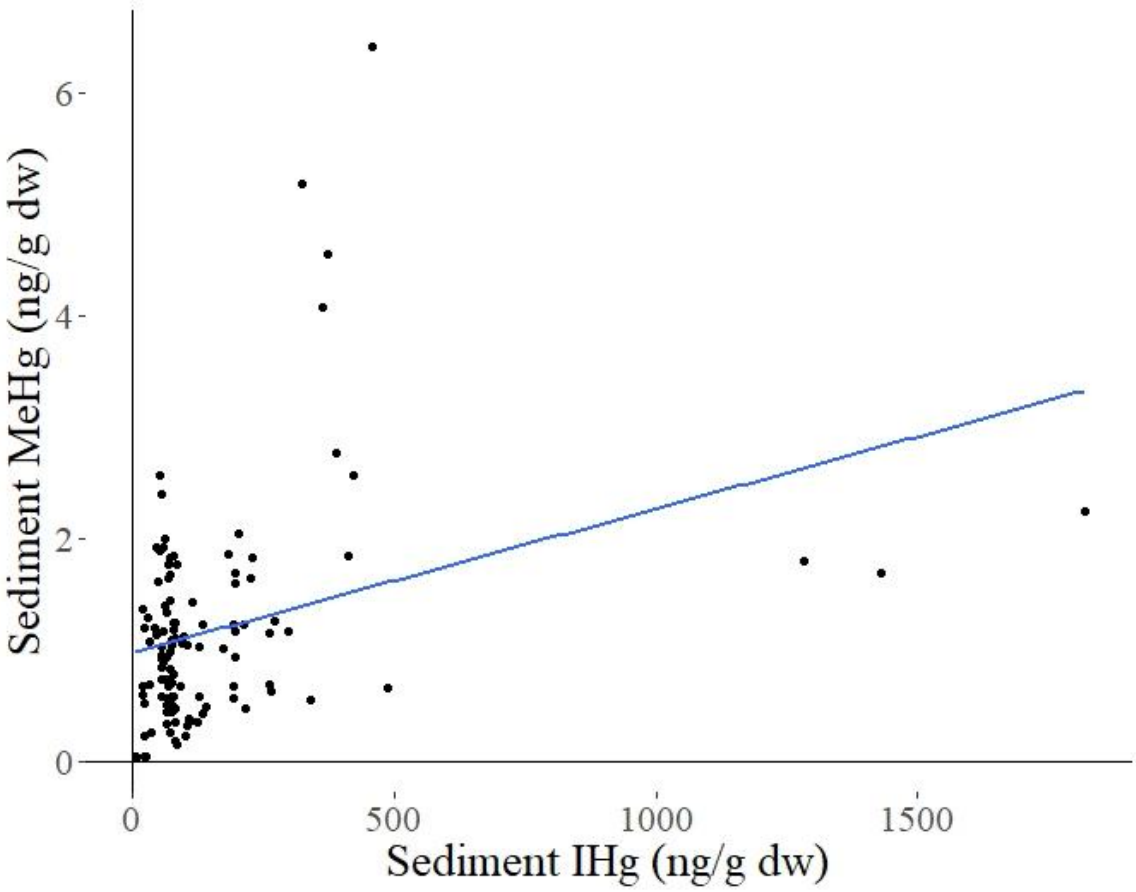

Figure 6: Linear regression of sediment MeHg vs sediment inorganic Hg. The relationship is not very strong but significant (R^2 = 0.1101 and p = 0.0002), likely influenced by the handful of high inorganic Hg sites found in the industrial bays. Despite this trend, the highest sediment MeHg was observed at sites with sediment inorganic Hg less than 500 ng/g dw, suggesting the high inorganic Hg sites that are likely point source contaminated could potentially mobilize Hg at a higher rate if current conditions change, such as the introduction of more carbon or reduce oxygenation in the overlying water.

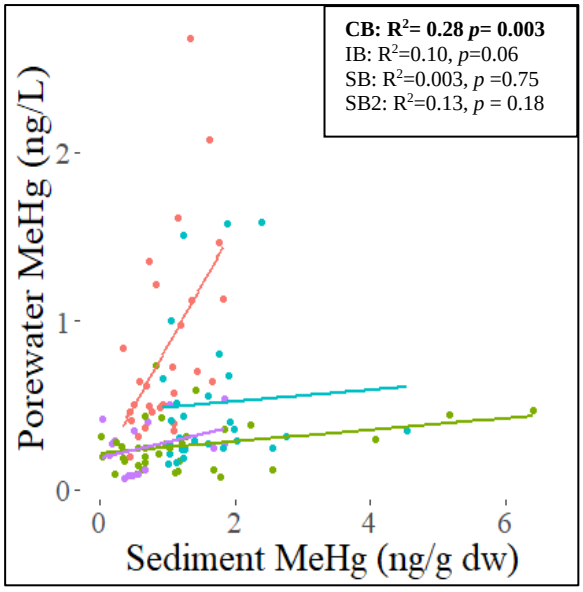

Figure 7: The relationship between porewater MeHg and sediment MeHg. If the amount of MeHg in the porewater was strictly a function of solid phase MeHg we would see a significant and strong relationship between these two concentrations, but because that is not the case. This suggests other factors, such as other porewater chemistry or solid phase characteristics could be more important for controlling partitioning of MeHg into the porewater.

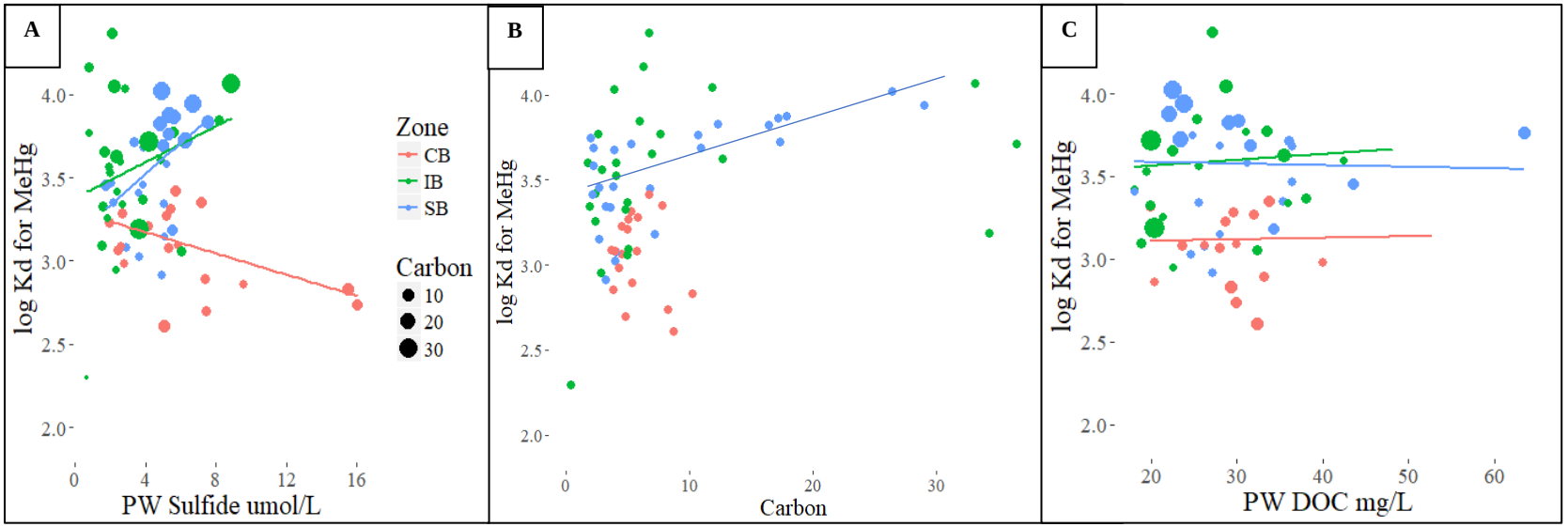

Figure 8: Log partitioning coefficient for MeHg plotted against porewater sulfide (A), sediment percent carbon (B), and porewater dissolved organic carbon (C). Size of bubbles corresponds to carbon and color represents habitat zone. There are significant negative relationship between porewater sulfide and log K_d in the claybays ($p = 0.006$, $R^2 = 0.25$) and a significant positive relationship between solid phase carbon and log K_d in the sheltered bays ($p < 0.001$, $R^2 = 0.46$).

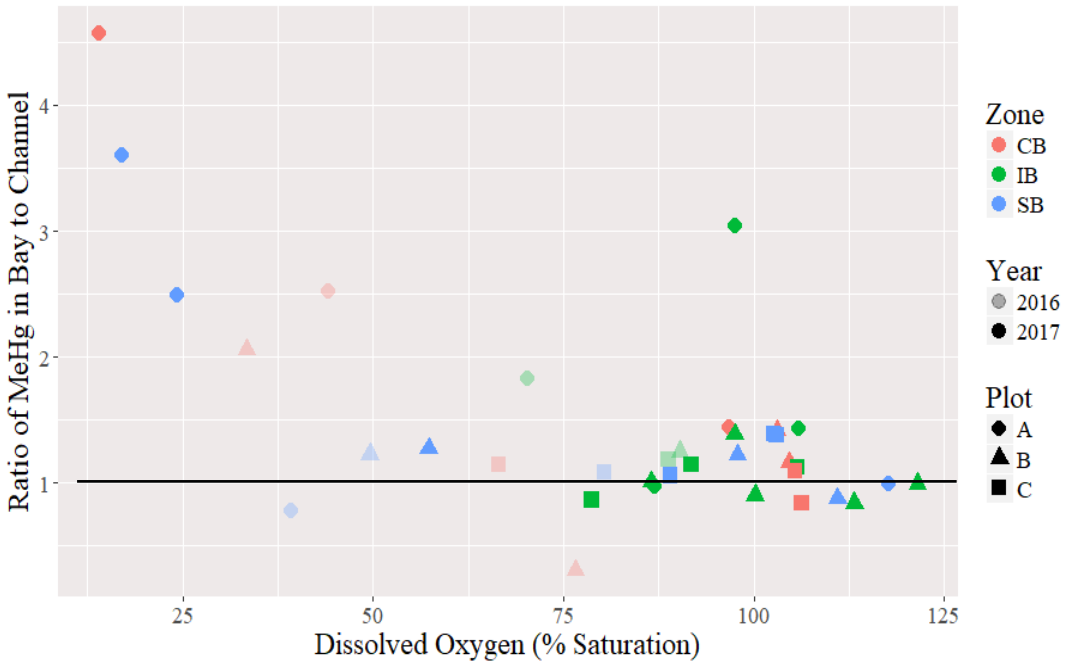

Figure 9: Ratio of embayment surface water MeHg versus dissolved oxygen. A line is drawn is a ratio of 1, which is where surface water MeHg is the same in the embayment and channel. Ratios greater than 1 mean MeHg is higher in the embayment than the channel and suggest a localized MeHg source, mostly likely from within in the embayment. Color represents habitat zone and shape represents plot. Lighter shaded points represent 2016 samples and darker points are 2017 samples. River flow was higher in 2016 than 2017.

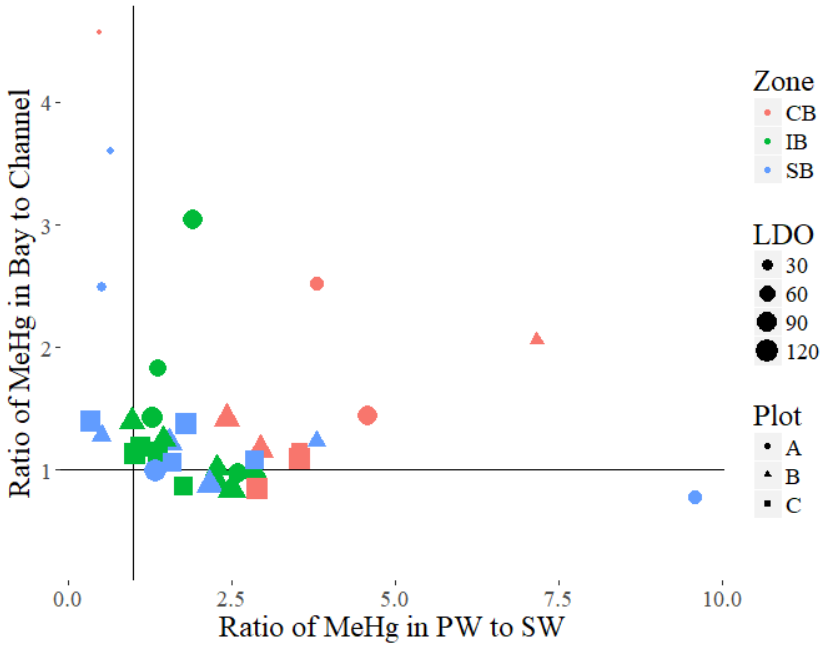

Figure 10: Comparison of bay to channel ratio (y-axis) and porewater to surface water ratio (x-axis). Lines have been added to show ratios of 1 for each ratio. Dots are colored according to habitat zone: sheltered bays (SB) are blue, industrial bays (IB) are green, and clay bays (CB) are red. The size of the dot corresponds to the dissolved oxygen, an indicator of isolation from main river channel. The plot is indicated by the shape: A is circles, B is triangles, and C is squares.

Table 1: Summary of sediment methylmercury (MeHg), Sediment inorganic mercury (iHg), sediment percent methylmercury, (Percent MeHg), sediment acid volatile sulfide (AVS), sediment 1 M HCL extractable iron (SEM), and sediment organic carbon. The average of n samples are presented with one standard deviation and coefficient of variatiton in parentheses

Habitat Zone	*n*	*MeHg [ng g $^{-1}$ dw]*	*iHg (ng g $^{-1}$ dw)*	*Percent MeHg*	*AVS (umol g $^{-1}$ dw)*	*SEM (umol g $^{-1}$ dw)*	*Organic carbon (%)*
Clay bay (CB)	30	1.0 ± 0.4 (0.44)	59.1 ± 20.1 (0.39)	2.0 ± 1.4 (0.73)	4.3 ± 4.5 (1.04)	189.4 ± 63. 5 (0.34)	5.8 ± 1.9 (0.34)
Industrial bay (IB)	42	1.2 ± 1.3 (1.10)	243.5 ± 393.0 (1.62)	1.1 ± 1.1 (1.01)	2.6 ± 3.1 (1.19)	137.5 ± 74.4 (0.54)	9.0 ± 10.4 (1.15)
Sheltered bay (SB)	30	1.6 ± 0.7 (0.46)	153.9 ± 107.4 (0.70)	1.8 ± 1.2 (0.73)	10.2 ± 9.4 (0.92)	200.3 ± 57.7 (0.29)	9.2 ± 7.9 (0.85)
Perch Lake (SB2)	18	0.7 ± 0.6 (0.83)	120.3 ± 54.3 (0.45)	0.6 ± 0.6 (0.96)	31.8 ± 26.6 (0.83)	193.6 ± 67.7 (0.35)	13.8 ± 7.2 (0.52)

Table 2: Summary of porewater chemistry presented as the average of n samples plus or minus one standard deviation including porewater MeHg (MeHg), porewater inorganic Hg, log Kd for both MeHg and inorganic Hg, porewater sulfide, and porewater dissolved organic carbon.

Habitat Zone	*n*	*MeHg (ng L^{-1})*	*Inorganic Hg (ng L^{-1})*	*MeHg $logK_d$*	*iHg $logK_d$*	*Porewater Sulfide (umol L^{-1})*	*DOC mg L^{-1}*
Clay bay (CB)	30	0.8 ± 0.6 (0.68)	2.0 ± 0.9 (0.47)	3.1 ± 0.2 (0.07)	4.5 ± 0.2 (0.05)	6.0 ± 3.5 (0.58)	30.3 ± 7.1 (0.23)
Industrial Bay (IB)	42	0.3 ± 0.1 (0.57)	3.0 ± 1.6 (0.51)	3.5 ± 0.5 (0.14)	4.7 ± 0.7 (0.16)	3.3 ± 2.1 (0.65)	28.4 ± 7.8 (0.27)
Sheltered bay (SB)	30	0.5 ± 0.4 (0.81)	1.7 ± 1.1 (0.61)	3.6 ± 0.3 (0.09)	4.9 ± 0.5 (0.09)	4.6 ± 1.4 (0.32)	30.6 ± 9.1 (0.30)
Perch Lake (SB2)	18	0.3 ± 0.2 (0.65)	1.1 ± 0.4 (0.38)	3.4 ± 0.5 (0.16)	5.0 ± 0.2 (0.04)	4.6 ± 3.2 (0.69)	25.7 ± 5.6 (0.22)

Table 3: This table shows which habitat types are significantly different ($p < 0.05$) across the five mercury related variables. The color of the shading indicates where significant differences occur, and the text in the box describes what the significant difference is. The sign next to the habitat type acronym indicates the "direction" of significance. For example, the sheltered bays had significantly higher sediment MeHg than the industrial bay and clay bay. This table is meant as a summary of the ANOVA analyses completed here and attempts to describe the mercury and geochemical "fingerprint" of the habitat zones of the SLRE.

	Clay Bay (CB)	Sheltered Bay (SB)	Industrial Bay (IB)
Sediment THg	SB >	CB <	
Sediment MeHg	SB >	IB <, CB<	< SB
Sediment AVS	SB >	IB <, CB <	SB >
Sediment %MeHg	IB <	IB <	CB >
Sediment Carbon		IB <	SB >
Porewater MeHg	SB <, IB <	> IB, CB <	SB >, CB >
MeHg K_d	IB <	IB <	SB >, CB >

Aiken, George R., Heileen Hsu-Kim, and Joseph N. Ryan. 2011. “Influence of Dissolved Organic Matter on the Environmental Fate of Metals, Nanoparticles, and Colloids.” *Environmental Science and Technology* 45 (8): 3196–3201. https://doi.org/10.1021/es103992s.

Alimi, Olubukola S., Jeffrey Farner Budarz, Laura M. Hernandez, and Nathalie Tufenkji. 2018. “Microplastics and Nanoplastics in Aquatic Environments: Aggregation, Deposition, and Enhanced Contaminant Transport.” *Environmental Science and Technology* 52 (4): 1704–24. https://doi.org/10.1021/acs.est.7b05559.

Bailey, Logan T., Carl P.J. Mitchell, Daniel R. Engstrom, Michael E. Berndt, Jill K. Coleman Wasik, and Nathan W. Johnson. 2017. “Influence of Porewater Sulfide on Methylmercury Production and Partitioning in Sulfate-Impacted Lake Sediments.” *Science of the Total Environment* 580: 1197–1204. https://doi.org/10.1016/j.scitotenv.2016.12.078.

Balcom, Prentiss H., Amina T. Schartup, Robert P. Mason, and Celia Y. Chen. 2015. “Sources of Water Column Methylmercury across Multiple Estuaries in the Northeast U.S.” *Marine Chemistry* 177: 721–30. https://doi.org/10.1016/j.marchem.2015.10.012.

Beck, Brian F., and Nathan W. Johnson. 2014. “Geochemical Factors Influencing the Production and Transport of Methylmercury in St. Louis River Estuary Sediment.” *Applied Geochemistry* 51: 44–54. https://doi.org/10.1016/j.apgeochem.2014.09.009.

Benoit, J.M. Jm, Cc C.C. Gilmour, A. Heyes, Rp Mason, and Cl Miller. 2003. “Geochemical and Biological Controls over Methylmercury Production and Degradation in Aquatic Ecosystems.” *ACS Symposium*. https://doi.org/10.1021/bk-2003-0835.ch019.

Benoit, Janina M., Cynthia C. Gilmour, Robert P. Mason, and Andrew Heyes. 1999. “Sulfide Controls on Mercury Speciation and Bioavailability to Methylating Bacteria in Sediment Pore Waters.” *Environmental Science and Technology* 33 (6): 951–57. https://doi.org/10.1021/es9808200.

Berndt, Michael, and Travis Bavin. 2009. “Sulfate and Mercury Chemistry of the St. Louis River in Northeastern Minnesota: A Report to the Minerals Coordinating Committee.” *Minnesota Department of Natural Resources, Division of Lands and Minerals*, 1–83.

Berndt, Michael E., and Travis K. Bavin. 2012. “Methylmercury and Dissolved Organic Carbon Relationships in a Wetland-Rich Watershed Impacted by Elevated Sulfate from Mining.” *Environmental Pollution* 161: 321–27. https://doi.org/10.1016/j.envpol.2011.06.006.

Bloom, Nicholas S. 1989. “Determination of Picogram Levels of Methylmercury by Aqueous Phase Ethylation, Followed by Cryogenic Gas Chromatography with Cold Vapour Atomic Fluorescence Detection.” *Canadian Journal of Fisheries and Aquatic Sciences* 46 (7): 1131–40. https://doi.org/10.1111/j.1468-2249.2011.00330.x.

Bloom, Nicolas S., Eve Preus, Jodie Katon, and Misti Hiltner. 2003. “Selective Extractions to Assess the Biogeochemically Relevant Fractionation of Inorganic Mercury in Sediments and Soils.” *Analytica Chimica Acta* 479 (2): 233–48. https://doi.org/10.1016/S0003-2670(02)01550-7.

Bower, Julia, Kaye S. Savage, Beth Weinman, Mark O. Barnett, William P. Hamilton, and Willie F. Harper. 2008. “Immobilization of Mercury by Pyrite (FeS2).” *Environmental Pollution* 156 (2): 504–14. https://doi.org/10.1016/j.envpol.2008.01.011.

Bravo, Andrea G., Jakob Zopfi, Moritz Buck, Jingying Xu, Stefan Bertilsson, Jeffra K. Schaefer, John Poté, and Claudia Cosio. 2018. “Geobacteraceae Are Important Members of Mercury-Methylating Microbial Communities of Sediments Impacted by Waste Water Releases.” *ISME Journal* 12 (3): 802–12. https://doi.org/10.1038/s41396-017-0007-7.

Brown, Steven D., Cynthia C. Gilmour, Amy M. Kucken, Judy D. Wall, Dwayne A. Elias, Craig C. Brandt, Mircea Podar, et al. 2011. “Genome Sequence of the Mercury-Methylating Strain Desulfovibrio Desulfuricans ND132.” *Journal of Bacteriology* 193 (8): 2078–79. https://doi.org/10.1128/JB.00170-11.

Cesário, Rute, Holger Hintelmann, Ricardo Mendes, Kevin Eckey, Brian Dimock, Beatriz Araújo, Ana Maria Mota, and João Canário. 2017. “Evaluation of Mercury Methylation and Methylmercury Demethylation Rates in Vegetated and Non-Vegetated Saltmarsh Sediments from Two Portuguese Estuaries.” *Environmental Pollution* 226: 297–307. https://doi.org/10.1016/j.envpol.2017.03.075.

Chen, Celia Y, Michele Dionne, Brandon M Mayes, Darren M Ward, Stefan Sturup, and Brian P Jackson.

2009. “Mercury Bioavailability and Bioaccumulation in Estuarine Food Webs in the Gulf of Maine Mercury Bioavailability and Bioaccumulation in Estuarine Food Webs in the Gulf of Maine.” *Environmental Science and Technology* 43 (6): 1804–10. https://doi.org/10.1021/es8017122.

Chételat, John, M Brian C Hickey, Alexandre J Poulain, Ashu Dastoor, Andrei Ryjkov, Donald Mcalpine, Karen Vanderwolf, et al. 2018. “Science of the Total Environment Spatial Variation of Mercury Bioaccumulation in Bats of Canada Linked to Atmospheric Mercury Deposition.” *Science of the Total Environment* 626: 668–77. https://doi.org/10.1016/j.scitotenv.2018.01.044.

Compeau, G C, and R Bartha. 1985. “Sulfate-Reducing Bacteria: Principal Methylators of Mercury in Anoxic Estuarine Sedimentt.” *Applied and Environmental Microbiology* 50 (2): 498–502.

Drenner, Ray W., Matthew M. Chumchal, Stephen P. Wente, Mandy McGuire, and S. Matthew Drenner. 2011. “Landscape-Level Patterns of Mercury Contamination of Fish in North Texas, USA.” *Environmental Toxicology and Chemistry* 30 (9): 2041–45. https://doi.org/10.1002/etc.589.

Eagles-Smith, Collin A., and Joshua T. Ackerman. 2014. “Mercury Bioaccumulation in Estuarine Wetland Fishes: Evaluating Habitats and Risk to Coastal Wildlife.” *Environmental Pollution* 193: 147–55. https://doi.org/10.1016/j.envpol.2014.06.015.

Eaton, A.D., L.S. Clesceri, E.W Rice, A.E. Greenbaerg, and M. A. H Franson. 2005. *Standard Methods for Examination of Water and Wastewater: Centennial Edition*. *American Public Health Association (APHA): Washington, DC, USA*. Vol. 21. https://doi.org/ISBN 9780875532356.

Eckley, Chris S., Todd P. Luxton, Jennifer Goetz, and John McKernan. 2017. “Water-Level Fluctuations Influence Sediment Porewater Chemistry and Methylmercury Production in a Flood-Control Reservoir.” *Environmental Pollution* 222: 32–41. https://doi.org/10.1016/j.envpol.2017.01.010.

Gerbig, Chase A., Christopher S. Kim, John P. Stegemeier, Joseph N. Ryan, and George R. Aiken. 2011. “Formation of Nanocolloidal Metacinnabar in Mercury-DOM-Sulfide Systems.” *Environmental Science and Technology* 45 (21): 9180–87. https://doi.org/10.1021/es201837h.

Gilmour, C C, G S Riedel, M C Ederington, J T Bell, J M Benoit, G a Gill, and Mary C Stordal. 1998.

"Methylmercury Concentrations and Production Rates across a Trophic Gradient in the Northern Everglades." *Biogeochemistry* 40: 327–45. https://doi.org/10.1023/A:1005972708616.

Gilmour, Cynthia, James Tyler Bell, Ally Bullock Soren, Georgia Riedel, Gerhardt Riedel, A. Dianne Kopec, and R. A. Bodaly. 2018. "Distribution and Biogeochemical Controls on Net Methylmercury Production in Penobscot River Marshes and Sediment." *Science of the Total Environment* 640–641: 555–69. https://doi.org/10.1016/j.scitotenv.2018.05.276.

Gilmour, Cynthia C., Elizabeth A. Henry, and Mitchell Ralph. 1992. "Sulfate Stimulation of Mercury Methylation in Freshwater Sediments." *Environmental Science and Technology* 26 (11): 2281–87. https://doi.org/10.1021/es00035a029.

Gilmour, Cynthia C., Mircea Podar, Allyson L. Bullock, Andrew M. Graham, Steven D. Brown, Anil C. Somenahally, Alex Johs, Richard A. Hurt, Kathryn L. Bailey, and Dwayne A. Elias. 2013. "Mercury Methylation by Novel Microorganisms from New Environments." *Environmental Science and Technology* 47 (20): 11810–20. https://doi.org/10.1021/es403075t.

Hall, B. D., G. R. Aiken, D. P. Krabbenhoft, M. Marvin-DiPasquale, and C. M. Swarzenski. 2008. "Wetlands as Principal Zones of Methylmercury Production in Southern Louisiana and the Gulf of Mexico Region." *Environmental Pollution* 154 (1): 124–34. https://doi.org/10.1016/j.envpol.2007.12.017.

Hammerschmidt, Chad R., and William F. Fitzgerald. 2004. "Geochemical Controls on the Production and Distribution of Methylmercury in Near-Shore Marine Sediments." *Environmental Science and Technology* 38 (5): 1487–95. https://doi.org/10.1021/es034528q.

———. 2008. "Sediment-Water Exchange of Methylmercury Determined from Shipboard Benthic Flux Chambers." *Marine Chemistry* 109 (1–2): 86–97. https://doi.org/10.1016/j.marchem.2007.12.006.

Hammerschmidt, Chad R., William F. Fitzgerald, Prentiss H. Balcom, and Pieter T. Visscher. 2008. "Organic Matter and Sulfide Inhibit Methylmercury Production in Sediments of New York/New Jersey Harbor." *Marine Chemistry* 109 (1–2): 165–82. https://doi.org/10.1016/j.marchem.2008.01.007.

Haynes, Kristine M., Evan S. Kane, Lynette Potvin, Erik A. Lilleskov, Randall K. Kolka, and Carl P.J. Mitchell. 2017. “Mobility and Transport of Mercury and Methylmercury in Peat as a Function of Changes in Water Table Regime and Plant Functional Groups.” *Global Biogeochemical Cycles* 31 (2): 233–44. https://doi.org/10.1002/2016GB005471.

Heim, W A, K H Coale, M Stephenson, K Y Choe, G A Gill, and C Foe. 2007. “Spatial and Habitat-Based Variations in Total and Methyl Mercury Concentrations in Surficial Sediments in the San Francisco Bay-Delta.” *Environmental Science & Technology* 41 (10): 3501–7. https://doi.org/10.1021/es0626483.

Hesterberg, Dean, Jeff W. Chou, Kimberly J. Hutchison, and Dale E. Sayers. 2001. “Bonding of HG(II) to Reduced Organic Sulfur in Humic Acid as Affected by S/Hg Ratio.” *Environmental Science and Technology* 35 (13): 2741–45. https://doi.org/10.1021/es001960o.

Hines, Neal A., Patrick L. Brezonik, and Daniel R. Engstrom. 2004. “Sediment and Porewater Profiles and Fluxes of Mercury and Methylmercury in a Small Seepage Lake in Northern Minnesota.” *Environmental Science and Technology* 38 (24): 6610–17. https://doi.org/10.1021/es0496672.

Hintelmann, H., and R. D. Evans. 1997. “Application of Stable Isotopes in Environmental Tracer Studies - Measurement of Monomethylmercury (CH 3 Hg +) by Isotope Dilution ICP-MS and Detection of Species Transformation.” *Fresenius’ Journal of Analytical Chemistry* 358 (3): 378–85. https://doi.org/10.1007/s002160050433.

Hoffman, Joel C., Gregory S. Peterson, Anne M. Cotter, and John R. Kelly. 2010. “Using Stable Isotope Mixing in a Great Lakes Coastal Tributary to Determine Food Web Linkages in Young Fishes.” *Estuaries and Coasts* 33 (6): 1391–1405. https://doi.org/10.1007/s12237-010-9295-0.

Hsu-Kim, Heileen, Katarzyna H Kucharzyk, Tong Zhang, and Marc A Deshusses. 2013. “Mechanisms Regulating Mercury Bioavailability for Methylating Microorganisms in the Aquatic Environment: A Critical Review.” *Environmental Science & Technology* 47: 2441–56. https://doi.org/10.1021/es304370g.

Hsu, Liang Ching, Ching Yi Huang, Yen Hsun Chuang, Ho Wen Chen, Ya Ting Chan, Heng Yi Teah, Tsan

Yao Chen, Chiung Fen Chang, Yu Ting Liu, and Yu Min Tzou. 2016. “Accumulation of Heavy Metals and Trace Elements in Fluvial Sediments Received Effluents from Traditional and Semiconductor Industries.” *Scientific Reports* 6 (101): 1–12. https://doi.org/10.1038/srep34250.

Hurley, James P., Janina M. Benoit, Christopher L. Babiarz, Martin M. Shafer, Anders W. Andren, John R.Sulli Van, Richard Hammond, and David A. Webb. 1995. “Influences of Watershed Characteristics on Mercury Levels in Wisconsin Rivers.” *Environmental Science and Technology* 29 (7): 1867–75. https://doi.org/10.1021/es00007a026.

Jackson, Brian, Vivien Taylor, R Arthur Baker, and Eric Miller. 2009. “Low-Level Mercury Speciation in Freshwaters by Isotope Dilution GC-ICP-MS Low-Level Mercury Speciation in Freshwaters by Isotope Dilution” 43 (7): 2463–69. https://doi.org/10.1021/es802656p.

Jeremiason, Jeff D, Daniel R Engstrom, Edward B Swain, Edward A Nater, Brian M Johnson, James E Almendinger, and Bruce A Monson. 2006. “Sulfate Addition Increases Methylmercury Production in an Experimental Wetland” 40 (12): 3800–3806. https://doi.org/10.1021/es0524144.

Johnson, Nathan W, Carl P J Mitchell, Daniel R Engstrom, Logan T Bailey, Jill K Coleman Wasik, and Michael E Berndt. 2016. “Methylmercury Production in a Chronically Sulfate-Impacted Sub-Boreal Wetland.” *Environmental Science-Processes & Impacts* 18 (6): 725–34. https://doi.org/10.1039/c6em00138f.

Kneer, Marissa L., Amber White, Kristofer R. Rolfhus, Jeffrey D. Jeremiason, Nathan W. Johnson, and Matthew Ginder-Vogel. 2020. “Impact of Dissolved Organic Matter on Porewater Hg and MeHg Concentrations in St. Louis River Estuary Sediments.” *ACS Earth and Space Chemistry* 4 (8): 1386–97. https://doi.org/10.1021/acsearthspacechem.0c00134.

LaFond-Hudson, Sophia, Nathan W. Johnson, John Pastor, and Brad Dewey. 2018. “Iron Sulfide Formation on Root Surfaces Controlled by the Life Cycle of Wild Rice (Zizania Palustris).” *Biogeochemistry* 141 (1): 95–106. https://doi.org/10.1007/s10533-018-0491-5.

Lamborg, C H, W F Fitzgerald, A W H Damman, J M Benoit, P H Balcom, and D R Engstrom. 2002. “Modern and Historic Atmospheric Mercury Fluxes in Both Hemispheres : Global and Regional

Mercury Cycling Implications" 16 (4). https://doi.org/10.1029/2001GB001847.

Landrum, Peter F., and Warren R. Faust. 1994. "The Role of Sediment Composition on the Bioavailability of Laboratory-Dosed Sediment-Associated Organic Contaminants to the Amphipod, Diporeia (Spp.)." *Chemical Speciation and Bioavailability* 6 (2–3): 85–92. https://doi.org/10.1080/09542299.1994.11083226.

Lepak, Ryan F., Runsheng Yin, David P. Krabbenhoft, Jacob M. Ogorek, John F. Dewild, Thomas M. Holsen, and James P. Hurley. 2015. "Use of Stable Isotope Signatures to Determine Mercury Sources in the Great Lakes." *Environmental Science and Technology Letters* 2 (12): 335–41. https://doi.org/10.1021/acs.estlett.5b00277.

Louis, Vincent L. St., John W. M. Rudd, Carol A. Kelly, Ken G. Beaty, Nicholas S. Bloom, and Robert J. Flett. 1994. "Importance of Wetlands as Sources of Methyl Mercury to Boreal Forest Ecosystems." *Canadian Journal of Fisheries and Aquatic Sciences* 51 (5): 1065–76. https://doi.org/10.1139/f94-106.

Manceau, Alain, Cyprien Lemouchi, Mironel Enescu, Anne Claire Gaillot, Martine Lanson, Valérie Magnin, Pieter Glatzel, et al. 2015. "Formation of Mercury Sulfide from Hg(II)-Thiolate Complexes in Natural Organic Matter." *Environmental Science and Technology* 49 (16): 9787–96. https://doi.org/10.1021/acs.est.5b02522.

McClain, Michael E., Elizabeth W. Boyer, C. Lisa Dent, Sarah E. Gergel, Nancy B. Grimm, Peter M. Groffman, Stephen C. Hart, et al. 2003. "Biogeochemical Hot Spots and Hot Moments at the Interface of Terrestrial and Aquatic Ecosystems." *Ecosystems* 6 (4): 301–12. https://doi.org/10.1007/s10021-003-0161-9.

Mehrotra, Anna, and David L Sedlak. 2005. "Decrease in Net Mercury Methylation Rates Following Iron Amendment to Anoxic Wetland Sediment Slurries" 39 (8): 2564–70. https://doi.org/10.1021/es049096d.

Mitchell, C P J, B a Branfireun, and R K Kolka. 2008. "Spatial Characteristics of n et Methylmercury Production Hot Spots in Peatlands." *Environmental Science & Technology* 42 (4): 1010–16.

Myrbo, A., E. B. Swain, N. W. Johnson, D. R. Engstrom, J. Pastor, B. Dewey, P. Monson, J. Brenner, M. Dykhuizen Shore, and E. B. Peters. 2017. “Increase in Nutrients, Mercury, and Methylmercury as a Consequence of Elevated Sulfate Reduction to Sulfide in Experimental Wetland Mesocosms.” *Journal of Geophysical Research: Biogeosciences* 122 (11): 2769–85. https://doi.org/10.1002/2017JG003788.

Parks, Jerry M, Alex Johs, Mircea Podar, Romain Bridou, Richard a. Hurt, Steven D. Smith, Stephen J Tomanicek, et al. 2013a. “The Genetic Basis for Bacterial Mercury Methylation.” *Science* 339 (6125): 1332–35. https://doi.org/10.1126/science.1230667.

Parks, Jerry M, Alex Johs, Mircea Podar, Romain Bridou, Richard A. Hurt, Steven D. Smith, Stephen J Tomanicek, et al. 2013b. “The Genetic Basis for Bacterial Mercury Methylation.” *Science* 220 (1968): 11–12. https://doi.org/10.1038/220173a0.

Petosa, Adamo R., Deb P. Jaisi, Ivan R. Quevedo, Menachem Elimelech, and Nathalie Tufenkji. 2010. “Aggregation and Deposition of Engineered Nanomaterials in Aquatic Environments: Role of Physicochemical Interactions.” *Environmental Science and Technology* 44 (17): 6532–49. https://doi.org/10.1021/es100598h.

Podar, Mircea, Cynthia C Gilmour, Craig C Brandt, Allyson Soren, Steven D Brown, Bryan R Crable, Anthony V Palumbo, Anil C Somenahally, and Dwayne A Elias. 2015. “Global Prevalence and Distribution of Genes and Microorganisms Involved in Mercury Methylation.” *Science Advances* 1 (9): 1–13. https://doi.org/10.1126/sciadv.1500675.

Poulin, Brett A., Joseph N. Ryan, Kathryn L. Nagy, Aron Stubbins, Thorsten Dittmar, William Orem, David P. Krabbenhoft, and George R. Aiken. 2017. “Spatial Dependence of Reduced Sulfur in Everglades Dissolved Organic Matter Controlled by Sulfate Enrichment.” *Environmental Science and Technology* 51 (7): 3630–39. https://doi.org/10.1021/acs.est.6b04142.

Rolfhus, Kristofer R., Britt D. Hall, Bruce A. Monson, Michael J. Paterson, and Jeffrey D. Jeremiason. 2011. “Assessment of Mercury Bioaccumulation within the Pelagic Food Web of Lakes in the Western Great Lakes Region.” *Ecotoxicology* 20 (7): 1520–29. https://doi.org/10.1007/s10646-011-

0733-y.

Schartup, Amina T, Prentiss H Balcom, and Robert P Mason. 2014. “Sediment-Porewater Partitioning, Total Sulfur, and Methylmercury Production in Estuaries.” *Environmental Science & Technologyl*. https://doi.org/10.1021/es403030d.

Seeberg-elverfeldt, Jens, Michael Schluter, Tomas Feseker, and Martin Kolling. 2005. “Rhizon Sampling of Porewaters near the Sediment-Water Interface of Aquatic Systems.” *Limnology and Oceanography-Methods* 3: 361–71.

SLRA. 2002. “Lower St . Louis River Habitat Plan.”

Sorensen, John, Mike Sydor, Hubert Huls, and Mike Costello. 2004. “Analyses of Lake Superior Seiche Activity for Estimating Effects on Pollution Transport in the St. Louis River Estuary under Extreme Conditions.” *Journal of Great Lakes Research* 30 (2): 293–300. https://doi.org/10.1016/S0380-1330(04)70347-0.

Tjerngren, I, T Karlsson, E. Björn, and U Skyllberg. 2012. “Potential Hg Methylation and MeHg Demethylation Rates Related to the Nutrient Status of Different Boreal Wetlands.” *Biogeochemistry* 108 (1–3): 335–50. https://doi.org/10.1007/s10533-011-9603-1.

Ullrich, S., T. Tanton, and S. Abdrashitova. 2001. “Mercury in the Aquatic Environment: A Review of Factors Affecting Methylation.” *Crit. Rev. Environ. Sci. Technol.* 31 (3): 241– 293.

Wasik, Jill K Coleman, Daniel R. Engstrom, Carl P.J. Mitchell, Ed B. Swain, Bruce A. Monson, S. J. Balogh, Jeff D Jeremiason, Brian A. Branfireun, Randall K. Kolka, and J. E. Almendinger. 2015. “The Effects of Hydrologic Fluctuation and Sulfate Regeneration on Mercury Cycling in an Experimental Peatland.” *Journal of Geophysical Research: Biogeosciences* 120: 1697–1715. https://doi.org/10.1002/2015JG002993.Received.

Wiener, J. G., B. C. Knights, M. B. Sandheinrich, J. D. Jeremiason, M. E. Brigham, D. R. Engstrom, L. G. Woodruff, W. F. Cannon, and S. J. Balogh. 2006. “Mercury in Soils, Lakes, and Fish in Voyageurs National Park (Minnesota): Importance of Atmospheric Deposition and Ecosystem Factors.”

Environmental Science and Technology 40 (20): 6261–68. https://doi.org/10.1021/es060822h.

Windham-Myers, Lisamarie, Mark Marvin-Dipasquale, David P. Krabbenhoft, Jennifer L. Agee, Marisa H. Cox, Pilar Heredia-Middleton, Carolyn Coates, and Evangelos Kakouros. 2009. "Experimental Removal of Wetland Emergent Vegetation Leads to Decreased Methylmercury Production in Surface Sediment." *Journal of Geophysical Research: Biogeosciences* 114 (3): 1–14. https://doi.org/10.1029/2008JG000815.

Appendix

Tables:

Figures

Special sections

Table S1: Description of site name, field code, habitat zone, plot, year visited, and GPS coordinates.

Site	Field Code	Habitat Zone	Plot	Year	Latitude	Longitude
Rask Bay	SB1	Sheltered Bay	A	2016	46.65709	-92.27025
Rask Bay	SB1	Sheltered Bay	B	2016	46.65635	-92.27013
Rask Bay	SB1	Sheltered Bay	C	2016	46.65500	-92.26928
Perch Lake	SB2	Sheltered Bay	A	2016/17	46.66063	-92.25483
Perch Lake	SB2	Sheltered Bay	B	2016/17	46.66039	-92.25443
Perch Lake	SB2	Sheltered Bay	C	2016/17	46.66054	-92.25345
North Bay	SB3	Sheltered Bay	A	2017	46.65347	-92.24356
North Bay	SB3	Sheltered Bay	B	2017	46.65293	-92.24207
North Bay	SB3	Sheltered Bay	C	2017	46.65311	-92.23934
Kingsbury Bay	KNG	Sheltered Bay	A	2016/17	46.72092	-92.18729
Kingsbury Bay	KNG	Sheltered Bay	B	2017	46.72040	-92.18691
Kingsbury Bay	KNG	Sheltered Bay	C	2017	46.71975	-92.18570
Pokegama	CB1	Clay Bay	A	2016/17	46.67795	-92.16632
Pokegama	CB1	Clay Bay	B	2016/17	46.67965	-92.16703
Pokegama	CB1	Clay Bay	C	2016/17	46.68061	-92.16642
Little Pokegama	CB2	Clay Bay	A	2017	46.66240	-92.19478
Little Pokegama	CB2	Clay Bay	B	2016/17	46.66289	-92.19453
Little Pokegama	CB2	Clay Bay	C	2017	46.66312	-92.19464
Clough Island	UEF	Industrial Bay	A	2016/17	46.71066	-92.18375
Clough Island	UEF	Industrial Bay	B	2016/17	46.71157	-92.18456
Clough Island	UEF	Industrial Bay	C	2016/17	46.71336	-92.18648
40th Ave West	IB1	Industrial Bay	A	2017	46.73895	-92.15433
40th Ave West	IB1	Industrial Bay	B	2017	46.73811	-92.15320
40th Ave West	IB1	Industrial Bay	C	2017	46.73835	-92.15146
Howard's Bay	IB2	Industrial Bay	A	2017	46.74162	-92.09428
Howard's Bay	IB2	Industrial Bay	B	2017	46.74104	-92.09467
Howard's Bay	IB2	Industrial Bay	C	2017	46.73632	-92.08875
Barker's Island	IB3	Industrial Bay	B	2017	46.71803	-92.05949
Lower Estuary Flat	LEF	Industrial Bay	B	2016/17	46.73804	-92.06155

Table S2: Description of sediment identification characteristics and geochemistry of each sediment replicate which was averaged into habitat zones for ANOVA analysis. Table includes habitat zone, site field code (see Table S1 for expanded site location description), plot, replicate, and year as sample identifiers. Geochemistry includes sediment methylmercury in ng/g dry weight (SMeHg), sediment total mercury in ng/g dry weight (STHg), sediment inorganic mercury (sediment total – sediment methylmercury) in ng/g dry weight (SIHg), sediment percent methylmercury (sediment methylmercury / sediment total mercury), sediment acid volatile sulfide from a 1 M HCl extraction in µmol/g dry weight (AVS), sediment simultaneously extracted iron present as ferrous iron from a 1 M HCl extraction in µmol/g dry weight (1 M Fe), molar ratio of AVS to 1 M extractable iron (AVS:Fe), and sediment percent carbon (Carbon).

Zone	Site	Plot	Replicate	Year	SMeHg	STHg	SIHg	SPMHg	AVS	1 M Fe	AVS:Fe	Carbon
CB	CB1	A	1	2016	0.74	54.02	53.28	1.36	9.41	226.68	0.04	8.28
CB	CB1	A	1	2017	0.67	68.35	67.68	0.98	3.84	187.84	0.02	8.42
CB	CB1	A	2	2016	0.82	72.47	71.64	1.14	23.35	268.14	0.09	10.25
CB	CB1	A	2	2017	0.73	64.43	63.70	1.13	9.04	250.98	0.04	8.66
CB	CB1	A	3	2016	0.34	80.94	80.60	0.42	6.70	209.20	0.03	8.68
CB	CB1	A	3	2017	0.44	65.69	65.25	0.67	7.13	204.25	0.03	7.81
CB	CB1	B	1	2016	1.63	67.67	66.04	2.41	2.94	251.13	0.01	5.38
CB	CB1	B	1	2017	0.58	53.57	52.99	1.08	1.90	172.45	0.01	6.11
CB	CB1	B	2	2016	1.77	70.62	68.85	2.51	6.75	192.23	0.04	5.76
CB	CB1	B	2	2017	0.94	56.47	55.53	1.66	0.79	162.03	0.00	5.08
CB	CB1	B	3	2016	1.44	72.38	70.94	1.99	3.26	267.19	0.01	5.32
CB	CB1	B	3	2017	0.89	56.77	55.88	1.57	0.85	240.46	0.00	5.15
CB	CB1	C	1	2016	1.10	82.67	81.57	1.33	1.88	297.70	0.01	5.84
CB	CB1	C	1	2017	0.57	78.68	78.11	0.72	0.80	241.52	0.00	6.91
CB	CB1	C	2	2016	0.47	80.06	79.59	0.59	7.29	144.74	0.05	4.53
CB	CB1	C	2	2017	0.44	73.40	72.96	0.60	0.44	198.46	0.00	4.29
CB	CB1	C	3	2016	0.78	78.80	78.02	0.99	0.75	140.45	0.01	4.49
CB	CB1	C	3	2017	1.09	76.81	75.72	1.42	0.34	178.63	0.00	7.34

CB	CB2	A	1	2017	1.20	22.18	20.98	5.41	3.61	162.83	0.02	3.71
CB	CB2	A	2	2017	0.59	18.34	17.75	3.22	0.42	138.73	0.00	2.62
CB	CB2	A	3	2017	1.36	18.54	17.18	7.34	7.15	161.09	0.04	4.01
CB	CB2	B	1	2016	1.83	73.64	71.81	2.49	0.93	143.90	0.01	4.96
CB	CB2	B	1	2017	1.09	74.09	73.00	1.47	4.31	128.28	0.03	5.97
CB	CB2	B	2	2016	1.16	59.98	58.82	1.94	5.46	381.87	0.01	3.83
CB	CB2	B	2	2017	1.67	70.74	69.07	2.36	6.63	147.82	0.04	6.76
CB	CB2	B	3	2016	1.33	64.40	63.07	2.07	2.91	144.53	0.02	4.85
CB	CB2	B	3	2017					5.70	120.45	0.05	6.17
CB	CB2	C	1	2017	0.51	22.55	22.04	2.26	0.56	99.97	0.01	4.10
CB	CB2	C	2	2017	0.69	30.60	29.91	2.25	0.17	100.19	0.00	2.90
CB	CB2	C	3	2017	1.07	31.75	30.68	3.37	4.36	118.47	0.04	2.01
IB	IB1	A	1	2017	1.18	77.07	75.89	1.53	0.28	76.79	0.00	5.99
IB	IB1	A	2	2017	1.20	42.19	40.99	2.84	2.14	60.10	0.04	6.77
IB	IB1	A	3	2017								9.26
IB	IB1	B	1	2017	0.23	23.11	22.88	1.00	0.67	87.64	0.01	2.38
IB	IB1	B	2	2017	0.26	35.07	34.81	0.74	0.53	100.10	0.01	4.09
IB	IB1	B	3	2017	0.67	17.48	16.81	3.83	1.34	93.31	0.01	6.66
IB	IB1	C	1	2017	1.12	97.63	96.51	1.15	1.31	80.86	0.02	11.84
IB	IB1	C	2	2017	0.88	58.37	57.49	1.51	0.71	76.19	0.01	12.69
IB	IB1	C	3	2017	2.56	54.31	51.75	4.71	2.56	84.18	0.03	15.85
IB	IB2	A	1	2017					1.15	59.46	0.02	1.95
IB	IB2	A	2	2017	1.28	30.39	29.11	4.21	2.61	79.48	0.03	4.07
IB	IB2	A	3	2017	0.84	56.60	55.76	1.48	1.46	83.74	0.02	5.01
IB	IB2	B	1	2017	0.57	125.18	124.61	0.46	2.04	95.22	0.02	1.83
IB	IB2	B	2	2017	0.68	261.43	260.75	0.26	2.10	173.01	0.01	2.81
IB	IB2	B	3	2017	0.37	108.07	107.70	0.34	1.35	78.67	0.02	1.98
IB	IB2	C	1	2017	0.62	265.48	264.86	0.23	0.56	229.58	0.00	3.61
IB	IB2	C	2	2017	1.16	296.92	295.76	0.39	0.25	332.62	0.00	3.90

IB	IB2	C	3	2017	0.54	338.60	338.06	0.16	0.82	172.59	0.00	2.61
IB	IB3	B	1	2017	1.79	1283.46	1281.67	0.14	0.87	207.06	0.00	6.74
IB	IB3	B	2	2017	1.68	1430.75	1429.07	0.12	3.60	209.58	0.02	6.25
IB	IB3	B	3	2017	2.24	1824.20	1821.96	0.12	1.25	85.19	0.01	7.66
IB	LEF	B	1	2016		169.15	169.15		1.97	224.23	0.00	
IB	LEF	B	1	2017	0.04	21.13	21.09	0.19	0.39	22.68	0.02	0.49
IB	LEF	B	2	2017	0.03	6.24	6.21	0.48	0.17	32.31	0.01	0.34
IB	LEF	B	3	2017	0.04	4.40	4.36	0.91	0.66	20.32	0.03	0.45
IB	UEF	A	1	2016	1.84	413.45	411.61	0.45	12.72	158.77	0.08	36.50
IB	UEF	A	1	2017	5.18	327.38	322.20	1.58				33.08
IB	UEF	A	2	2016	0.66	488.99	488.33	0.14	2.50	217.24	0.01	34.25
IB	UEF	A	2	2017	6.42	462.53	456.11	1.39	9.31	161.83	0.06	33.04
IB	UEF	A	3	2016					8.54	159.78	0.05	30.34
IB	UEF	A	3	2017	4.08	364.80	360.72	1.12	11.04	169.98	0.06	31.07
IB	UEF	B	1	2016	0.32	102.28	101.96	0.31	0.84	198.54	0.00	5.07
IB	UEF	B	1	2017	1.04	104.15	103.11	1.00	3.13	47.23	0.07	10.42
IB	UEF	B	2	2016	0.66	90.38	89.72	0.74				4.10
IB	UEF	B	2	2017	1.22	134.24	133.02	0.91	4.47	211.94	0.02	6.95
IB	UEF	B	3	2016	0.91	56.29	55.38	1.62	2.60	318.73	0.01	4.83
IB	UEF	B	3	2017	1.43	113.89	112.46	1.26	7.16	151.64	0.05	6.16
IB	UEF	C	1	2016	0.34	65.94	65.60	0.51	0.22	231.94	0.00	2.35
IB	UEF	C	1	2017	0.56	67.93	67.37	0.82	0.41	151.86	0.00	5.02
IB	UEF	C	2	2016	0.25	71.49	71.24	0.35	0.67	160.42	0.00	2.81
IB	UEF	C	2	2017	0.57	73.88	73.31	0.77	0.69	128.42	0.01	2.38
IB	UEF	C	3	2016	0.98	72.68	71.69	1.35	5.30	198.28	0.03	2.92
IB	UEF	C	3	2017	0.50	74.47	73.97	0.67	1.79	154.48	0.01	2.63
SB	KNG	A	1	2016	1.91	59.94	58.03	3.19	4.35	233.46	0.02	6.84
SB	KNG	A	1	2017	1.83	230.57	228.74	0.79	9.31	222.72	0.04	17.86
SB	KNG	A	2	2016	1.13	46.45	45.32	2.44	4.91	300.09	0.02	3.20

SB	KNG	A	2	2017	1.25	272.36	271.11	0.46	36.55	277.92	0.13	17.40
SB	KNG	A	3	2016	1.61	47.63	46.02	3.38	4.33	197.27	0.02	3.79
SB	KNG	A	3	2017	1.14	261.18	260.04	0.44	9.50	184.03	0.05	17.18
SB	KNG	B	1	2017	2.56	422.96	420.40	0.61	2.69	233.20	0.01	26.43
SB	KNG	B	2	2017	4.55	376.44	371.89	1.21	20.80	228.97	0.09	27.92
SB	KNG	B	3	2017	2.76	392.01	389.25	0.70	14.22	230.38	0.06	29.01
SB	KNG	C	1	2017	1.22	192.51	191.29	0.63	3.56	205.42	0.02	5.31
SB	KNG	C	2	2017	1.17	196.85	195.68	0.59	3.28	226.98	0.01	5.70
SB	KNG	C	3	2017	0.93	195.79	194.86	0.47	5.25	367.27	0.01	5.35
SB	SB1	A	1	2016	2.40	56.33	53.93	4.26	6.18	196.17	0.03	7.15
SB	SB1	A	2	2016	1.92	45.81	43.89	4.19	9.99	148.46	0.07	3.87
SB	SB1	A	3	2016	1.88	53.74	51.86	3.50	2.39	176.06	0.01	4.02
SB	SB1	B	1	2016	1.06	94.47	93.42	1.12	0.70	79.20	0.01	3.97
SB	SB1	B	2	2016	1.23	80.49	79.25	1.53	8.09	83.12	0.10	3.19
SB	SB1	B	3	2016	1.76	84.92	83.17	2.07	2.60	187.11	0.01	3.64
SB	SB1	C	1	2016	0.94	65.18	64.24	1.43	3.98	162.25	0.02	2.66
SB	SB1	C	2	2016	1.99	62.74	60.74	3.18	17.16	145.88	0.12	2.04
SB	SB1	C	3	2016	1.40	61.57	60.18	2.27	8.70	229.28	0.04	2.24
SB	SB2	A	1	2016	0.70	74.94	74.24	0.94	90.34	336.42	0.27	13.18
SB	SB2	A	1	2017	0.49	140.41	139.92	0.35	1.49	101.54	0.01	30.11
SB	SB2	A	2	2016	1.84	79.94	78.10	2.30	40.00	296.34	0.13	12.70
SB	SB2	A	2	2017	1.85	184.89	183.04	1.00	4.93	99.22	0.05	28.63
SB	SB2	A	3	2016	0.18	79.94	79.77	0.22	17.27	174.53	0.10	11.60
SB	SB2	A	3	2017	1.69	196.80	195.11	0.86	22.61	118.58	0.19	26.03
SB	SB2	B	1	2016		122.59	122.59		26.41	243.47	0.11	11.30
SB	SB2	B	1	2017	0.47	214.80	214.33	0.22	20.63	176.28	0.12	13.19
SB	SB2	B	2	2016	1.03	56.04	55.01	1.83				11.58
SB	SB2	B	2	2017	0.56	192.67	192.11	0.29	21.10	220.29	0.10	16.47
SB	SB2	B	3	2016	0.04	25.06	25.02	0.16	25.72	152.56	0.17	11.65

SB	SB2	B	3	2017	0.67	191.57	190.90	0.35	10.63	191.52	0.06	15.94
SB	SB2	C	1	2016	0.22	100.78	100.56	0.22	64.60	216.92	0.30	8.85
SB	SB2	C	1	2017	0.42	134.70	134.28	0.31	20.55	151.63	0.14	7.07
SB	SB2	C	2	2016	0.50	64.40	63.90	0.78				8.89
SB	SB2	C	2	2017	0.36	109.47	109.11	0.33	5.66	125.61	0.05	3.83
SB	SB2	C	3	2016	0.14	82.49	82.34	0.17	84.77	272.97	0.31	8.60
SB	SB2	C	3	2017	0.35	124.72	124.37	0.28	52.07	219.03	0.24	7.77
SB	SB3	A	1	2017	1.23	211.18	209.95	0.58	24.14	231.24	0.10	16.40
SB	SB3	A	2	2017	1.03	128.65	127.62	0.80	31.49	254.03	0.12	10.94
SB	SB3	A	3	2017	1.01	172.22	171.21	0.59	27.73	228.08	0.12	12.29
SB	SB3	B	1	2017	1.60	195.34	193.74	0.82	19.64	175.48	0.11	10.72
SB	SB3	B	2	2017	2.04	202.99	200.95	1.01	3.10	174.58	0.02	9.44
SB	SB3	B	3	2017	1.64	226.92	225.28	0.72	10.84	145.21	0.07	10.95
SB	SB3	C	1	2017	1.04	76.08	75.04	1.37	2.70	153.84	0.02	2.28
SB	SB3	C	2	2017	1.24	77.19	75.95	1.61	5.23	165.08	0.03	2.74
SB	SB3	C	3	2017	1.06	75.16	74.10	1.41	2.19	167.17	0.01	2.16

Table S3: Description of porewater identification characteristics and geochemistry of each porewater replicate, which was averaged into habitat zones for ANOVA analysis. Table includes habitat zone, site field code (see Table S1 for expanded site location description), plot, replicate, and year as sample identifiers. Geochemistry includes porewater methylmercury in ng/L (PWMeHg), porewater total mercury in ng/L (PWTHg), porewater inorganic mercury (porewater total – porewater methylmercury) in ng/L dry weight (PWIHg), dissolved organic carbon in mg/L (PWDOC), porewater sulfate in mg/L (PWSulfate), porewater sulfide in μmol/L (PWSulfide), log of sediment porewater-sediment partitioning coefficient for methylmercury (log K_d MeHg), and log of sediment porewater-sediment partitioning coefficient for inorganic mercury (log K_d IHg).

Zone	Site	Plot	Replicate	Year	PWMeHg	PWTHg	PWIHg	PWDOC	PWSulfate	PWSulfide	Log K_d MeHg	Log K_d IHg
CB	CB1	A	1	2016	1.35	3.79	2.44	30.04	0.26	16.06	2.74	4.34
CB	CB1	A	1	2017	0.37	2.34	1.97	37.97		5.89	3.26	4.54
CB	CB1	A	2	2016	1.22	3.15	1.93	29.35	0.30	15.46	2.83	4.57
CB	CB1	A	2	2017	0.49	2.48	1.99	52.75	0.30	6.39	3.17	4.51
CB	CB1	A	3	2016	0.83	2.61	1.78	32.31	0.19	5.07	2.61	4.66
CB	CB1	A	3	2017	0.20	1.83	1.63	33.76	0.80	7.19	3.35	4.60
CB	CB1	B	1	2016	2.08	4.11	2.03	33.17	0.07	7.34	2.90	4.51
CB	CB1	B	1	2017	0.64			34.36	0.46	4.61	2.96	
CB	CB1	B	2	2016	1.47	2.79	1.32	23.64	0.17	5.31	3.08	4.72
CB	CB1	B	2	2017	0.50	4.87	4.37	32.00	0.58	5.19	3.27	4.10
CB	CB1	B	3	2016	0.70	1.37	0.67	19.87	0.30	5.43	3.32	5.02
CB	CB1	B	3	2017	0.48	3.75	3.26	31.85	0.33	2.26	3.27	4.23
CB	CB1	C	1	2016	0.57	3.27	2.70	29.62		2.69	3.28	4.48
CB	CB1	C	1	2017	0.31	2.02	1.70	34.57	0.35	5.37	3.26	4.66
CB	CB1	C	2	2016	0.40	2.48	2.07	27.99		2.41	3.07	4.58
CB	CB1	C	2	2017	0.46	2.37	1.90	40.09		2.76	2.98	4.58
CB	CB1	C	3	2016	0.46	3.23	2.77	28.61	0.12	1.93	3.23	4.45
CB	CB1	C	3	2017	0.39	5.12	4.73	38.95		2.39	3.45	4.20
CB	CB2	A	1	2017	0.97	2.02	1.05	30.05		5.83	3.09	4.30
CB	CB2	A	2	2017						4.46		
CB	CB2	A	3	2017	1.12	2.20	1.08	26.33		2.57	3.08	4.20

CB	CB2	B	1	2016	1.13	3.01	1.88	20.56	0.11	4.13	3.21	4.58
CB	CB2	B	1	2017	0.35	1.38	1.04	24.14	0.35	3.87	3.50	4.85
CB	CB2	B	2	2016	1.61	3.93	2.31	20.40	0.09	9.56	2.86	4.41
CB	CB2	B	2	2017	0.64	1.97	1.33			5.70	3.42	4.72
CB	CB2	B	3	2016	2.68	4.05	1.38		0.19	7.44	2.70	4.66
CB	CB2	B	3	2017	0.65	1.75	1.10	22.81	0.16	8.31		
CB	CB2	C	1	2017	0.50					6.41	3.01	
CB	CB2	C	2	2017	0.61	1.91	1.29	26.27		12.46	3.05	4.36
CB	CB2	C	3	2017	0.73	2.09	1.36	25.13		4.80	3.17	4.35
IB	IB1	A	1	2017	0.17	5.45	5.28	25.37	0.53	8.16	3.85	4.16
IB	IB1	A	2	2017								
IB	IB1	A	3	2017								
IB	IB1	B	1	2017	0.09	1.74	1.66	18.06		2.33	3.42	4.14
IB	IB1	B	2	2017						3.11		
IB	IB1	B	3	2017	0.16					1.98	3.62	
IB	IB1	C	1	2017	0.10	4.37	4.26	28.80		2.26	4.04	4.35
IB	IB1	C	2	2017	0.21	4.34	4.13	35.54		2.33	3.62	4.14
IB	IB1	C	3	2017	0.12					1.26	4.33	
IB	IB2	A	1	2017						2.15		
IB	IB2	A	2	2017	0.32					4.84	3.60	
IB	IB2	A	3	2017	0.74	2.02	1.29	32.36		6.00	3.06	4.64
IB	IB2	B	1	2017	0.14	2.32	2.18	42.46		2.56	3.60	4.76
IB	IB2	B	2	2017	0.25	3.25	3.00	48.14	0.17	3.63	3.44	4.94
IB	IB2	B	3	2017	0.17	5.33	5.16	35.96		2.69	3.34	4.32
IB	IB2	C	1	2017	0.11	3.61	3.50	29.72	0.39	4.20	3.74	4.88
IB	IB2	C	2	2017	0.11	2.99	2.89	28.93		2.83	4.03	5.01
IB	IB2	C	3	2017	0.09	3.10	3.00	31.03		0.76	3.77	5.05
IB	IB3	B	1	2017	0.08	3.03	2.96	27.17		2.13	4.37	5.64
IB	IB3	B	2	2017	0.11	3.95	3.84			0.74	4.17	5.57

IB	IB3	B	3	2017	0.38			33.55	0.15	5.62	3.77	
IB	LEF	B	1	2016	0.26	3.13	2.87	42.47		2.22		4.73
IB	LEF	B	1	2017								
IB	LEF	B	2	2017	0.31	6.59	6.27			3.39	1.91	3.00
IB	LEF	B	3	2017	0.19	2.54	2.35			0.67	2.30	3.27
IB	UEF	A	1	2016	0.36	2.47	2.12	20.07	0.29	4.20	3.71	5.29
IB	UEF	A	1	2017	0.44	0.81	0.36		0.34	8.81	4.07	5.95
IB	UEF	A	2	2016	0.43	2.71	2.28	20.43	0.29	3.67	3.19	5.33
IB	UEF	A	2	2017	0.47	2.21	1.74	26.13	1.49	7.67	4.14	5.42
IB	UEF	A	3	2016	0.31	2.71	2.40	20.80	0.21	3.33		
IB	UEF	A	3	2017	0.29			22.90	0.56	8.93	4.14	
IB	UEF	B	1	2016	0.26	4.40	4.15	18.85		1.48	3.10	4.39
IB	UEF	B	1	2017	0.25			35.38		1.69	3.62	
IB	UEF	B	2	2016	0.20	2.74	2.54	19.49	12.97	2.02	3.53	4.55
IB	UEF	B	2	2017	0.27	0.31	0.04	22.54	6.38	1.67	3.65	6.54
IB	UEF	B	3	2016	0.43	3.49	3.06	19.88	9.68	1.54	3.33	4.26
IB	UEF	B	3	2017	0.58	2.27	1.68	25.10	5.63	3.22	3.39	4.82
IB	UEF	C	1	2016	0.19	7.18	6.99	21.33	12.59	1.81	3.26	3.97
IB	UEF	C	1	2017	0.24			38.11		3.83	3.37	
IB	UEF	C	2	2016	0.28	4.48	4.20	22.57		2.30	2.95	4.23
IB	UEF	C	2	2017				39.12	3.13	3.22		
IB	UEF	C	3	2016	0.27	3.54	3.28	25.67		1.93	3.56	4.34
IB	UEF	C	3	2017				37.29	5.99	2.31		
SB	KNG	A	1	2016	0.67	1.74	1.07	43.61	0.10	1.76	3.45	4.74
SB	KNG	A	1	2017	0.24	1.07	0.83	22.12		5.35	3.87	5.44
SB	KNG	A	2	2016	0.51	1.42	0.91	35.45	0.09	2.20	3.35	4.70
SB	KNG	A	2	2017	0.24	1.65	1.42	23.55		6.24	3.72	5.28
SB	KNG	A	3	2016	0.56	1.56	1.00	36.44	0.09	2.04	3.46	4.66
SB	KNG	A	3	2017	0.16	1.55	1.40			5.59	3.87	5.27

SB	KNG	B	1	2017	0.24	1.45	1.21	22.57		4.93	4.02	5.54
SB	KNG	B	2	2017	0.35	2.12	1.77	23.24		6.44	4.12	5.32
SB	KNG	B	3	2017	0.32	1.80	1.49	23.88		6.69	3.94	5.42
SB	KNG	C	1	2017	0.24	2.10	1.86	36.01		3.33	3.71	5.01
SB	KNG	C	2	2017	0.30	2.94	2.64			5.26	3.59	4.87
SB	KNG	C	3	2017				43.39		2.57		
SB	SB1	A	1	2016	1.59	4.81	3.23	34.38	0.17	5.56	3.18	4.22
SB	SB1	A	2	2016	0.40	3.43	3.03	36.51	0.13	3.89	3.68	4.16
SB	SB1	A	3	2016	1.57	4.27	2.70	26.25		2.91	3.08	4.28
SB	SB1	B	1	2016	1.00	2.57	1.57	24.64	0.21	3.65	3.02	4.77
SB	SB1	B	2	2016	1.51	2.97	1.46	27.24	0.13	4.94	2.91	4.73
SB	SB1	B	3	2016	0.80	2.45	1.65	25.62	0.07	5.06	3.34	4.70
SB	SB1	C	1	2016	0.66	2.59	1.93	27.94	0.10	5.07	3.15	4.52
SB	SB1	C	2	2016	0.36	6.13	5.77	24.82	0.14	6.30	3.75	4.02
SB	SB1	C	3	2016	0.29	2.57	2.28	27.96	0.05	3.89	3.69	4.42
SB	SB2	A	1	2016	0.40	1.24	0.84	23.58	0.14	1.35	3.25	4.95
SB	SB2	A	1	2017	0.09	2.27	2.18	29.13		9.39	3.76	4.81
SB	SB2	A	2	2016	0.27	0.96	0.70	26.93	0.15	2.20	3.84	5.05
SB	SB2	A	2	2017	0.53	1.87	1.33	23.46	1.47	8.96	3.54	5.14
SB	SB2	A	3	2016	0.27	1.03	0.75	23.31	0.19	1.30	2.81	5.02
SB	SB2	A	3	2017	0.24	1.84	1.60	24.76		13.67	3.84	5.09
SB	SB2	B	1	2016	0.69	2.03	1.34	33.45	0.06	2.00		4.96
SB	SB2	B	1	2017	0.08	1.01	0.93	32.91	0.30	3.63	3.77	5.36
SB	SB2	B	2	2016	0.50	1.63	1.13	34.59	0.09	3.72	3.31	4.69
SB	SB2	B	2	2017	0.10	1.61	1.51	25.62		2.89	3.77	5.10
SB	SB2	B	3	2016	0.42	1.54	1.12	33.83	0.07	1.93	1.98	4.35
SB	SB2	B	3	2017	0.12	1.51	1.39	23.14	0.57	2.00	3.76	5.14
SB	SB2	C	1	2016	0.29	1.17	0.88	19.09	0.16	3.89	2.88	5.06
SB	SB2	C	1	2017	0.08	0.96	0.88	17.52		6.44	3.72	5.18

SB	SB2	C	2	2016	0.35	0.81	0.46	19.33	0.47	4.98	3.16	5.14
SB	SB2	C	2	2017	0.06	0.91	0.84	17.25	0.45	5.65	3.75	5.11
SB	SB2	C	3	2016	0.20	0.81	0.61		0.18	4.56	2.85	5.13
SB	SB2	C	3	2017				28.82		4.69		
SB	SB3	A	1	2017	0.18	0.87	0.68	29.06	0.21	4.80	3.83	5.49
SB	SB3	A	2	2017	0.21	1.03	0.82	31.56	0.39	4.96	3.69	5.19
SB	SB3	A	3	2017	0.15	1.11	0.96	30.25	0.89	7.54	3.83	5.25
SB	SB3	B	1	2017	0.27	1.85	1.58	63.43		5.28	3.76	5.09
SB	SB3	B	2	2017	0.29	0.67	0.38	25.34	0.32	3.56	3.85	5.72
SB	SB3	B	3	2017								
SB	SB3	C	1	2017	0.27	2.03	1.76	31.19	0.56	5.15	3.59	4.63
SB	SB3	C	2	2017	0.43					3.85	3.46	
SB	SB3	C	3	2017	0.41	1.92	1.51	18.13		3.57	3.41	4.69

Table S4: Description of surface water chemistry sample identification and geochemistry of site. Table includes habitat zone, site field code (see Table S1 for expanded site location description), plot, and year as sample identifiers. Chemistry includes dissolved oxygen in percent saturation (LDO), surface water methylmercury in ng/L (MeHg), and surface water sulfate in mg/L (Sulfate).

Zone	Site	Plot	Year	LDO	MeHg	Sulfate
CB	CB1	A	2016	44.1	0.35	0.86
CB	CB1	A	2017	14	0.73	9.00
CB	CB1	B	2016	33.4	0.29	0.95
CB	CB1	B	2017	104.7	0.18	5.87
CB	CB1	C	2016	66.5	0.16	1.63
CB	CB1	C	2017	106.3	0.13	5.39
CB	CB2	A	2017	96.7	0.23	14.19
CB	CB2	B	2016	76.6	0.04	1.60
CB	CB2	B	2017		0.23	8.26
CB	CB2	C	2017	105.4	0.17	5.32
CHN	CHN	A	2016	100.1	0.22	12.25
CHN	CHN	A	2017	111	0.15	5.88
CHN	CHN	B	2016	94.8	0.14	11.26
CHN	CHN	B	2017	96	0.16	6.15
CHN	CHN	C	2016		0.26	10.70
CHN	CHN	C	2017	98.4	0.09	8.87
IB	IB1	A	2017	105.9	0.13	
IB	IB1	B	2017	97.5	0.13	8.34
IB	IB1	C	2017	91.8	0.10	9.05
IB	IB2	A	2017	97.6	0.10	9.28
IB	IB2	B	2017	100.2	0.08	9.31
IB	IB2	C	2017	105.8	0.10	14.08
IB	IB3	B	2017	113.2	0.08	10.95
IB	LEF	B	2017	121.5	0.09	8.69
IB	UEF	A	2017	87	0.15	9.02
IB	UEF	B	2017	86.6	0.16	5.47
IB	UEF	C	2017	78.7	0.14	6.21
SB	KNG	A	2016		0.31	4.92
SB	KNG	A	2017	117.7	0.16	8.56
SB	KNG	B	2017	111	0.14	6.46
SB	KNG	C	2017	89	0.17	8.76
SB	SB1	A	2016	39.2	0.17	3.60
SB	SB1	B	2016	49.6	0.26	5.38
SB	SB1	C	2016	80.4	0.23	9.05
SB	SB2	A	2016		0.35	16.97

SB	SB2	A	2017	17.1	0.54	6.35
SB	SB2	B	2016		0.22	9.22
SB	SB2	B	2017	57.3	0.19	5.97
SB	SB2	C	2016		0.20	8.76
SB	SB2	C	2017	102.6	0.21	6.39
SB	SB3	A	2017	24.2	0.37	14.17
SB	SB3	B	2017	97.9	0.18	8.87
SB	SB3	C	2017	103	0.21	9.56
UEF	UEF	A	2016	70.3	0.26	7.70
UEF	UEF	B	2016	90.3	0.18	10.59
UEF	UEF	C	2016	88.8	0.17	10.43

Table S5: Summary of all depth discrete data for sediment and porewater. All depth discrete data was collected during the 2016 sampling season. Units: sediment methylmercury in ng/g dry weight (MeHg), sediment total mercury in ng/g dry weight (THg), sediment inorganic mercury (sediment total – sediment methylmercury) in ng/g dry weight (IHg), sediment percent methylmercury (sediment methylmercury / sediment total mercury), sediment acid volatile sulfide from a 1 M HCl extraction in µmol/g dry weight (AVS), methylation rate potential in fraction of total inorganic mercury methylated per day (Kmeth), porewater methylmercury in ng/L (MeHg), porewater total mercury in ng/L (THg), porewater inorganic mercury (porewater total – porewater methylmercury) in ng/L dry weight (IHg), dissolved organic carbon in mg/L (DOC), porewater sulfate in mg/L (Sulfate), and porewater sulfide in µmol/L (Sulfide).

		Sediment Solid						**Porewater**				
Site	Depth	AVS	THg	Ihg	MeHg	%MeHg	Kmeth	THg	MeHg	Sulfate	Sulfide	DOC
CB1A	0-2 cm	9.41	80.67	79.83	0.63	0.83	0.00	3.79	1.35	0.26	16.06	30.04
CB1A	2-4 cm	4.56	60.90					3.48	0.85		3.76	28.81
CB1A	4-8 cm	20.82								0.12	11.62	29.07
CB1B	0-2 cm	2.94	81.93	80.55	1.38	1.69	0.00	1.00	2.08	0.07	7.34	33.17
CB1B	2-4 cm	4.23	90.89					2.95	0.97	0.02	7.11	44.72
CB1B	4-8 cm	4.39								0.11	9.17	17.76
CB1C	0-2 cm	1.88	93.93	93.14	0.78	0.83	0.00	3.27	0.57	0.02	2.69	29.62
CB1C	2-4 cm	3.56	95.82					2.79	0.35	0.03	4.96	28.49
CB1C	4-8 cm	4.58								0.15	2.83	21.20
CB2B	0-2 cm	0.93	77.01	75.57	1.44	1.86	0.00	3.01	1.13	0.11	4.13	20.56
CB2B	2-4 cm	16.97						2.09	1.02	0.25	1.80	20.00
CB2B	4-8 cm	28.37						4.99	0.25		0.93	
CHNA	0-2 cm	0.17	19.02	19.05	0.10	0.46	0.00	6.75	1.70	0.99	2.46	32.30
CHNA	2-4 cm	0.20	24.09					4.30	0.64	0.13	2.31	36.96
CHNA	4-8 cm	0.43						3.23	0.55	0.04	1.17	23.32
CHNB	0-2 cm	0.20	46.27	46.03	0.25	0.53	0.00	6.64	0.41	3.86	1.89	38.33
CHNB	2-4 cm	0.25	42.19					3.92	0.84	0.33	2.56	56.67
CHNB	4-8 cm	0.25								2.31	4.13	39.95
CHNC	0-2 cm	0.15	126.96	126.43	0.53	0.42	0.00	2.28	0.21	7.74	0.80	24.78
CHNC	2-4 cm	0.25	143.51					4.53	0.32	2.13	1.63	28.92

CHNC	4-8 cm	6.00								0.12	2.54	32.38
KNG	0-2 cm	4.35	59.90	58.35	1.55	2.58	0.00	1.74	0.67	0.10	1.76	43.61
KNG	2-4 cm	1.39	57.95					2.27	0.49	0.11	1.80	46.11
KNG	4-8 cm	4.91								0.07	2.64	31.49
LEF	0-2 cm	1.97	169.15					3.13	0.26	0.89	2.22	
LEF	2-4 cm	12.24	161.70					3.03	0.21		1.09	
LEF	4-8 cm	6.11	158.26								1.76	
UEFA	0-2 cm	12.72	509.82	525.17	1.25	0.25	0.00	2.99	0.31	0.29	4.20	20.07
UEFA	2-4 cm	5.27	624.99					2.47	0.36	0.23	2.57	20.09
UEFA	4-8 cm	23.68						2.03	0.26	0.70	4.91	20.80
UEFB	0-2 cm	0.84	96.81	96.18	0.63	0.76	0.00	4.40	0.26		1.48	18.85
UEFB	2-4 cm	6.42						3.83	0.39		1.35	25.92
UEFB	4-8 cm	9.28						3.49	0.42	1.09	4.78	24.56
UEFC	0-2 cm	0.22	81.71	81.35	0.36	0.44	0.00	7.18	0.19	12.59	1.81	21.33
UEFC	2-4 cm	1.32	69.31					4.95	0.50	3.09	1.70	31.24
UEFC	4-8 cm	4.91								2.13	4.78	23.65
SB2A	0-2 cm	90.34	90.35	59.35	0.88	1.39	0.00	0.96	0.27	0.14	1.35	23.58
SB2A	2-4 cm	38.84	89.32					1.30	0.29	0.12	1.72	31.37
SB2A	4-8 cm	326.70								0.23	2.41	25.25
SB2B	0-2 cm	26.41	139.09	138.79	0.53	0.38	0.00	2.03	0.69	0.06	2.00	33.45
SB2B	2-4 cm	35.02	138.20					1.88	0.57	0.23	4.83	34.25
SB2B	4-8 cm	144.59								0.32	5.76	27.66
SB2C	0-2 cm	64.60	105.43	105.14	0.29	0.26	0.00	1.17	0.29	0.16	3.89	19.09
SB2C	2-4 cm	81.86	97.91					1.23	0.31	0.28	1.76	16.71
SB2C	4-8 cm	175.79								0.12	3.87	16.28
SB1A	0-2 cm	6.18	60.62	58.55	2.07	3.42	0.00	4.81	1.59	0.17	5.56	34.38
SB1A	2-4 cm	1.91	52.51					7.43	1.53		4.76	67.17
SB1A	4-8 cm	0.33						4.14	0.72		3.54	36.51
SB1B	0-2 cm	0.70	101.07	99.87	1.19	1.19	0.00	2.57	1.00	0.21	3.65	24.64

SB1B	2-4 cm	5.43	106.12					2.19	0.44	0.06	4.57	22.64
SB1B	4-8 cm	18.56						3.01	0.33	0.14	5.93	21.14
SB1C	0-2 cm	3.98	73.69	72.25	1.44	1.97	0.00	2.59	0.66	0.10	5.07	27.94
SB1C	2-4 cm	3.60	76.72					2.77	0.66	0.09	6.37	25.47
SB1C	4-8 cm	13.89						1.84	0.46	0.08	5.26	24.09

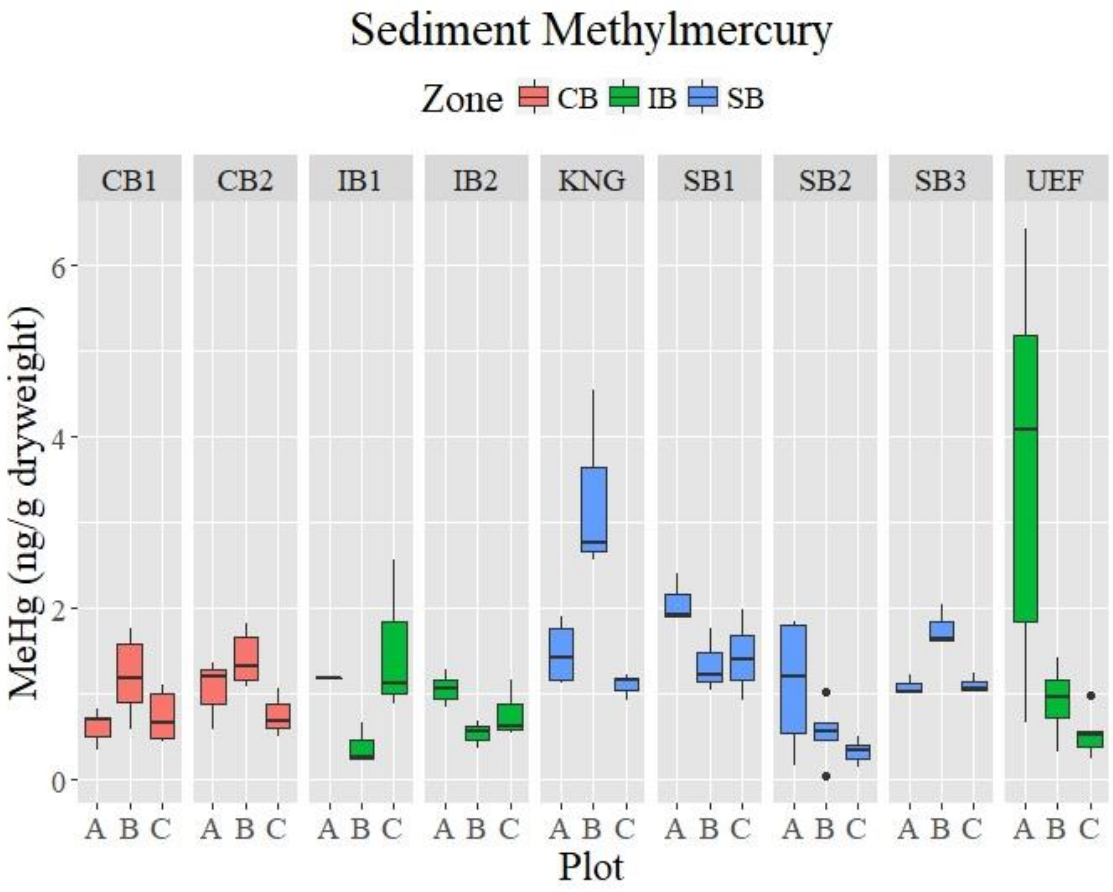

Figure S1: Sediment Methylmercury by individual sites (see Table S1 for more description of sites) and plot (separated within each site) and colored by habitat zone.

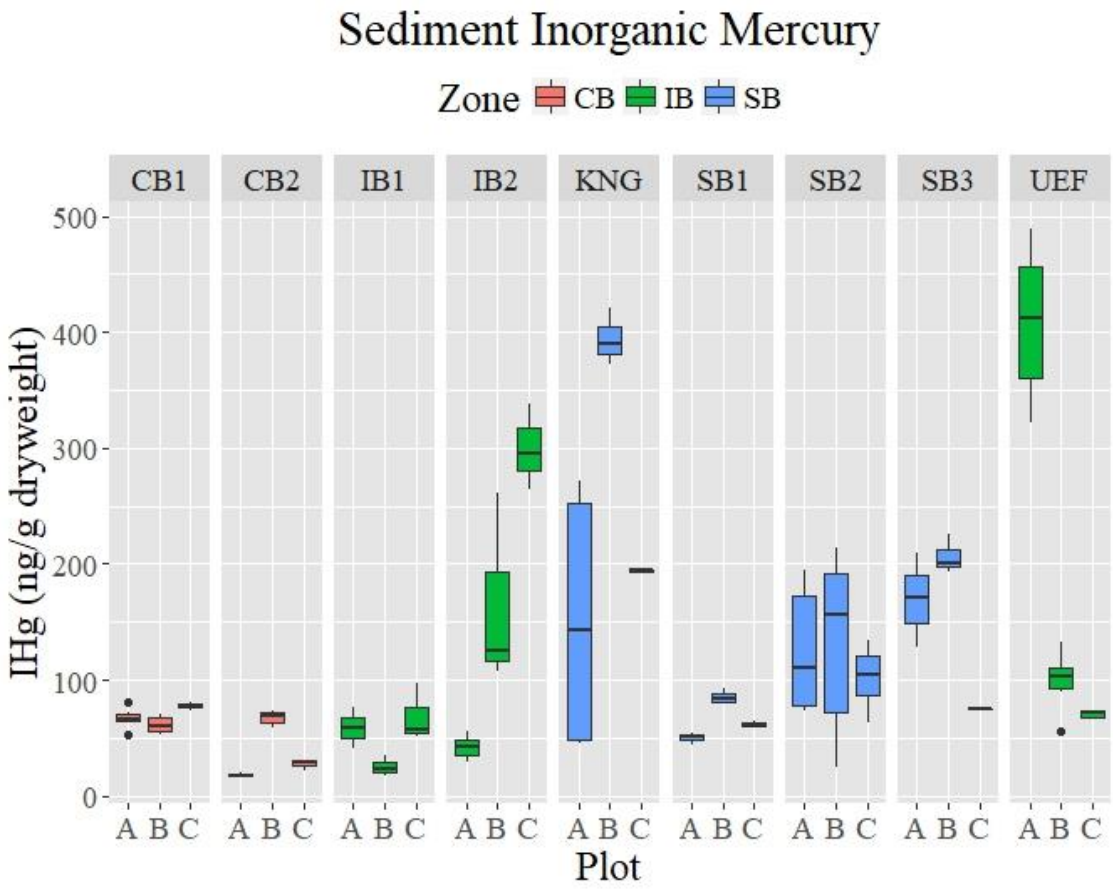

Figure S2: Sediment Inorganic Mercury by individual sites (see Table S1 for more description of sites) and plot (separated within each site) and colored by habitat zone.

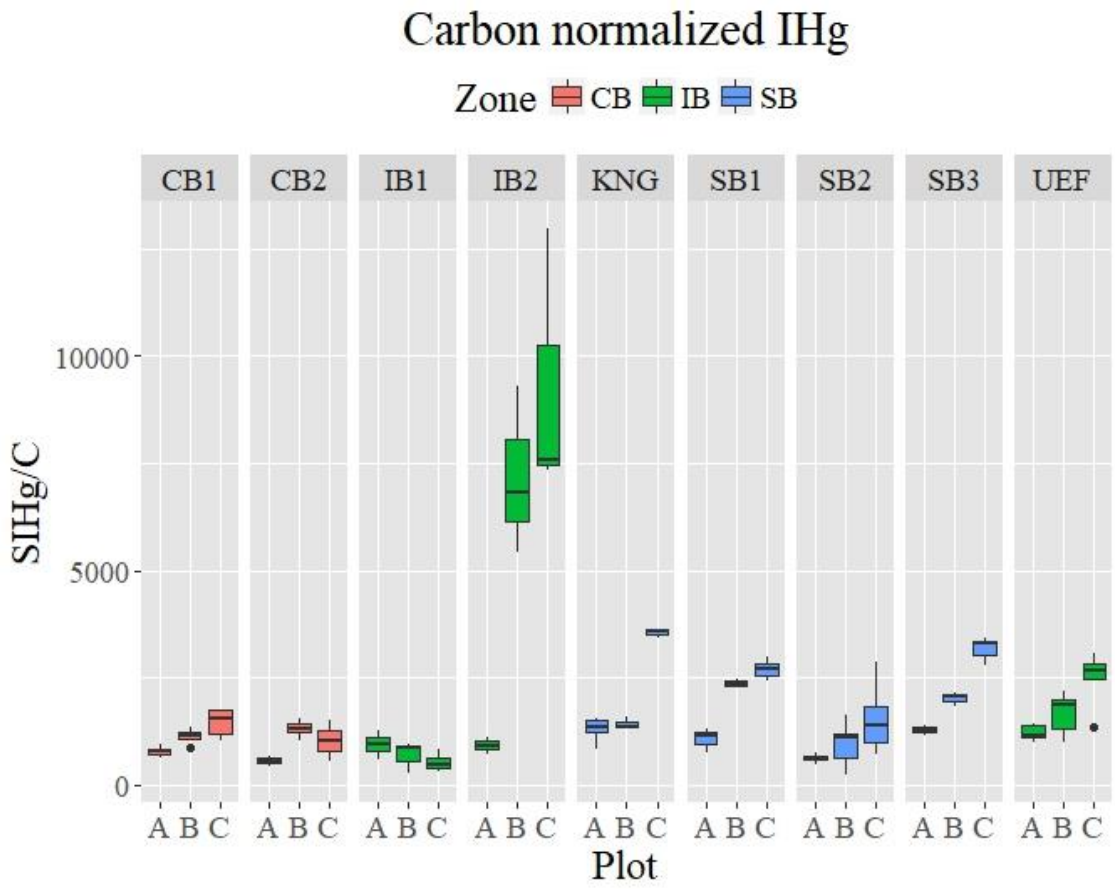

Figure S3: Sediment Inorganic Mercury normalized by sediment carbon for individual sites (see Table S1 for more description of sites) and plot (separated within each site) and colored by habitat zone.

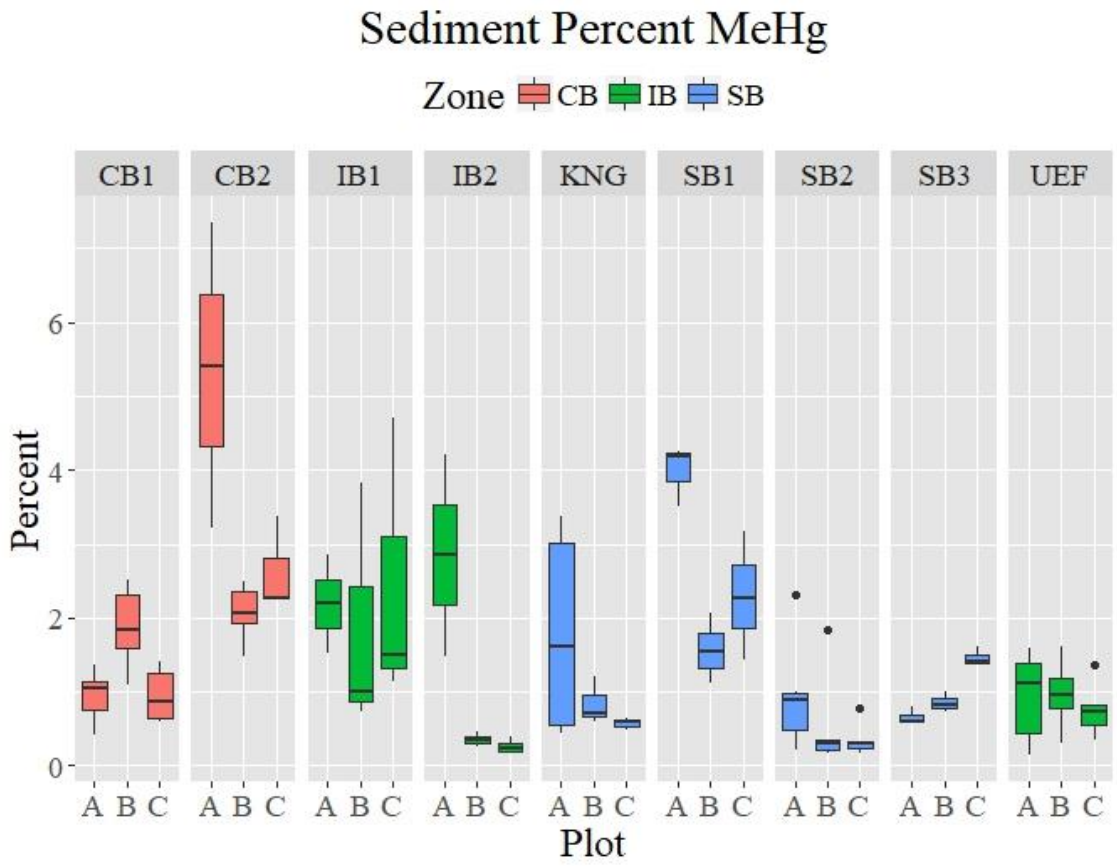

Figure S4: Sediment Percent Methylmercury by individual sites (see Table S1 for more description of sites) and plot (separated within each site) and colored by habitat zone.

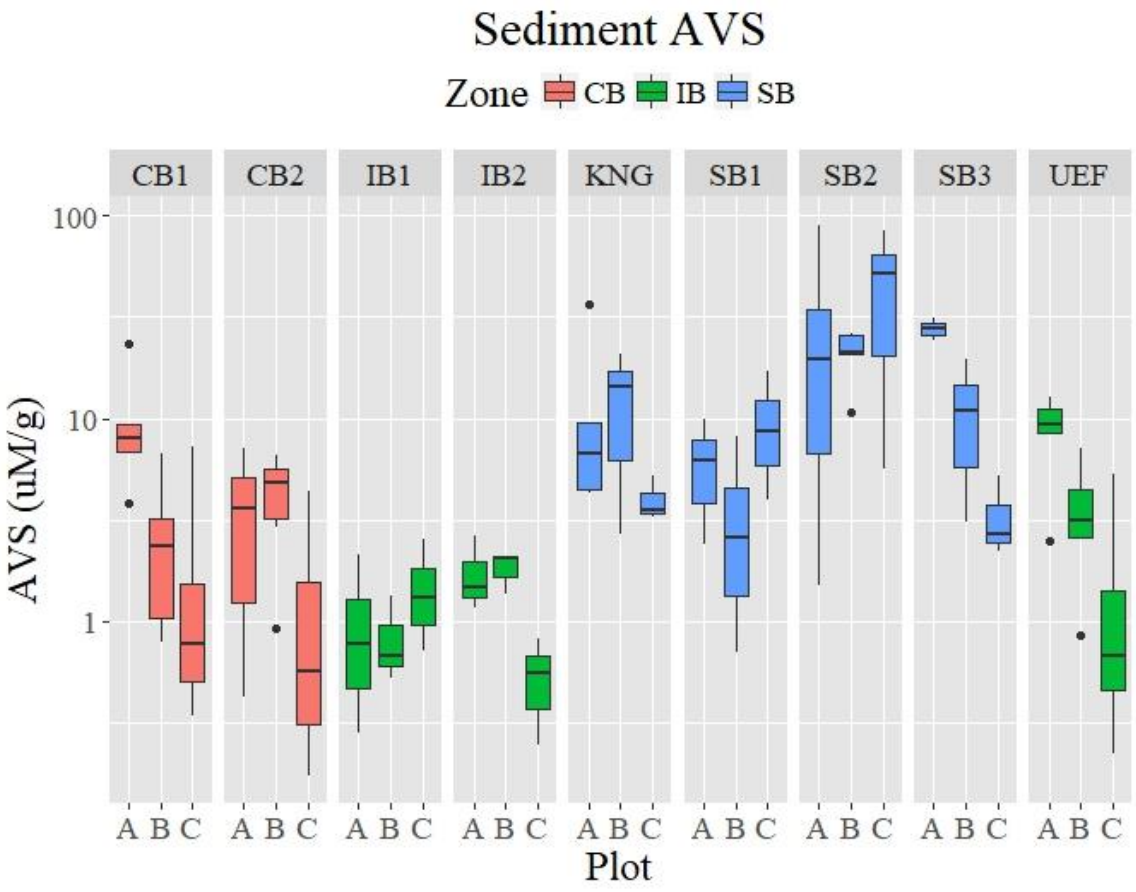

Figure S5: Sediment AVS by individual sites (see Table S1 for more description of sites) and plot (separated within each site) and colored by habitat zone. Concentration is presented in a log scale.

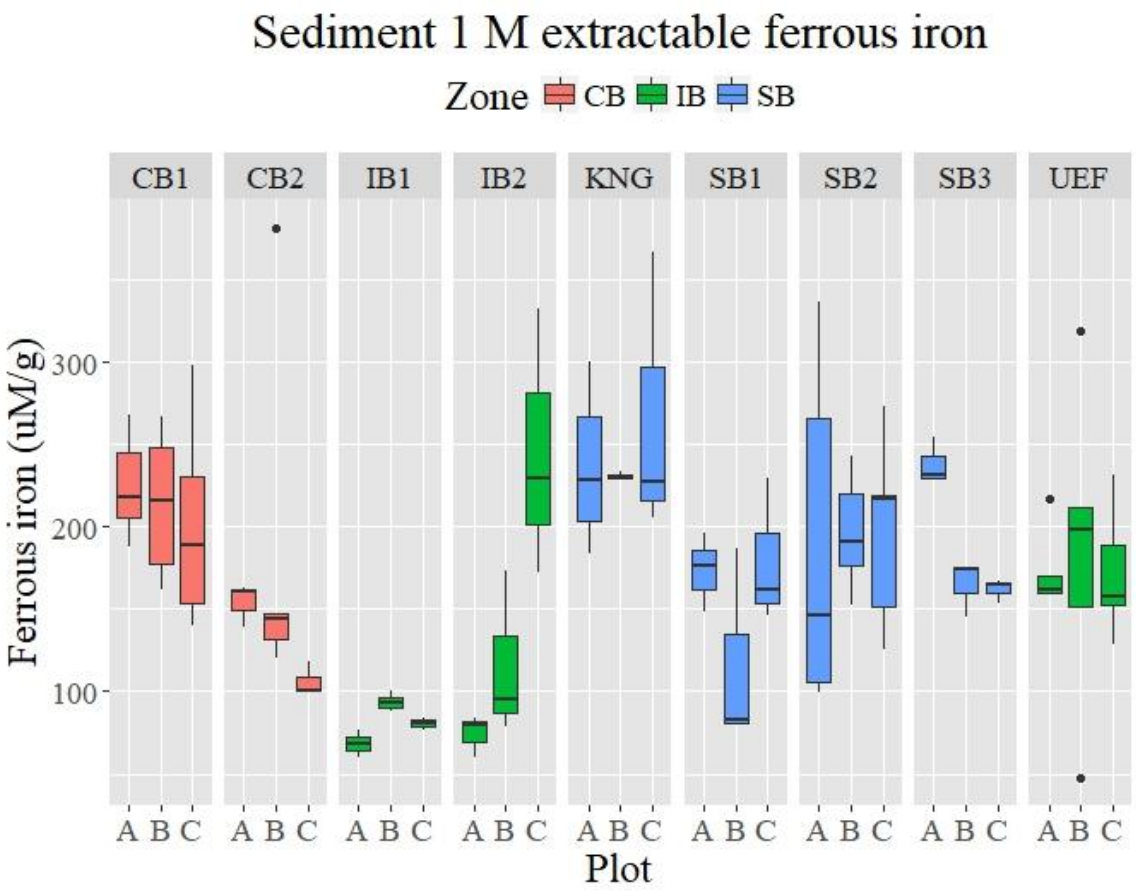

Figure S6: Sediment 1M acid extractable iron by individual sites (see Table S1 for more description of sites) and plot (separated within each site) and colored by habitat zone.

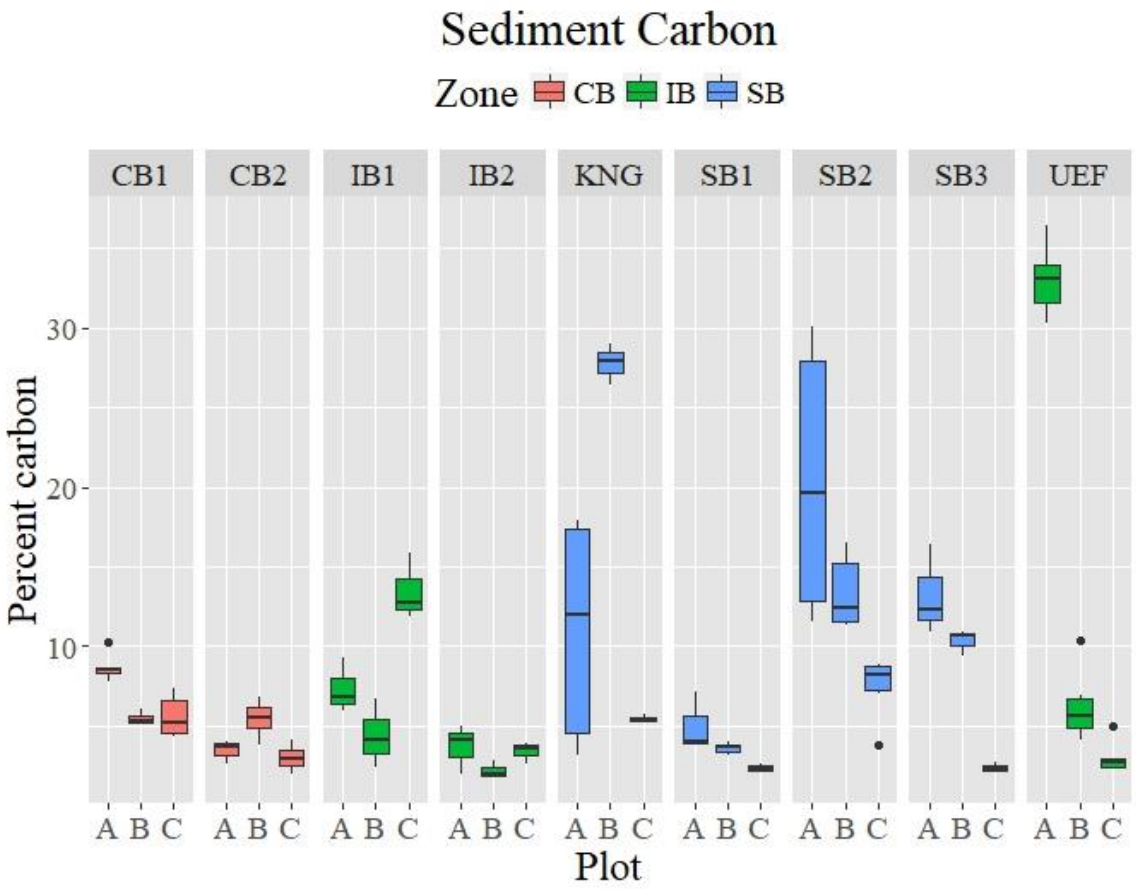

S7: Sediment percent carbon by individual sites (see Table S1 for more description of sites) and plot (separated within each site) and colored by habitat zone.

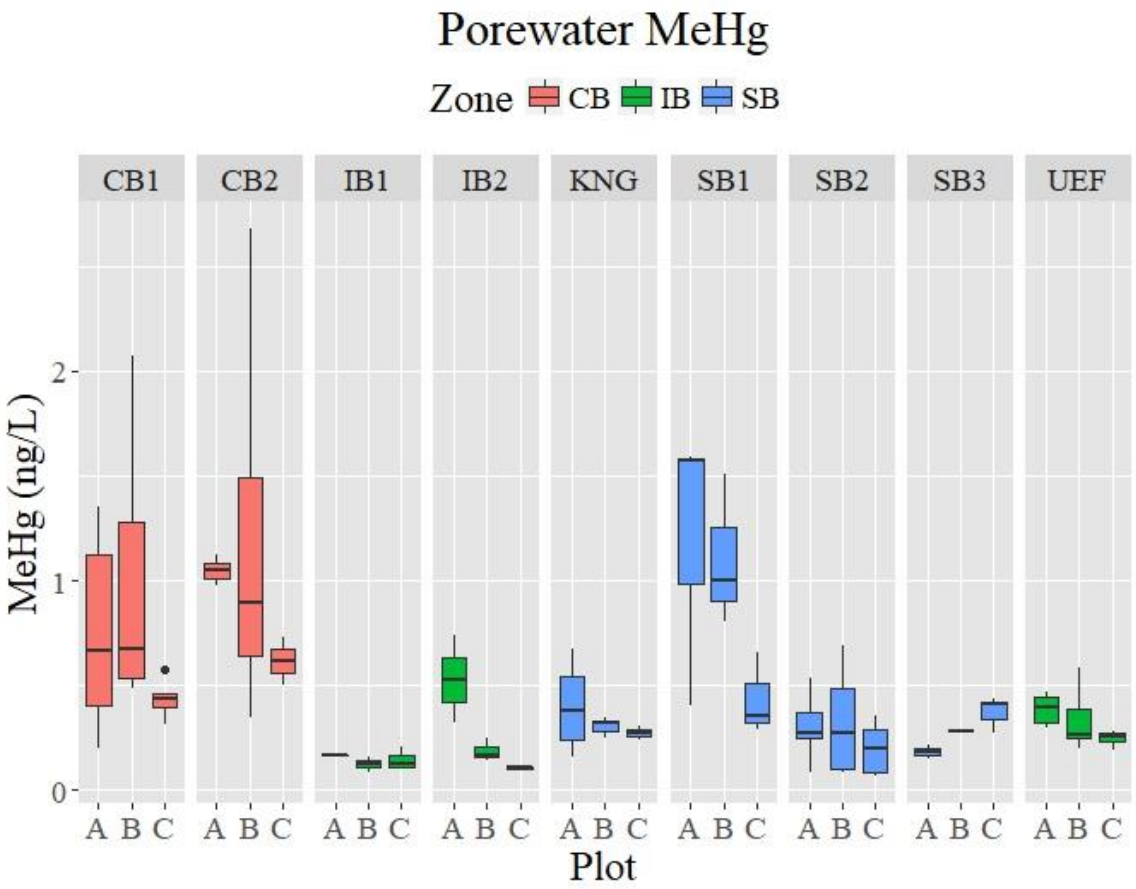

Figure S8: Porewater methylmercury by individual sites (see Table S1 for more description of sites) and plot (separated within each site) and colored by habitat zone

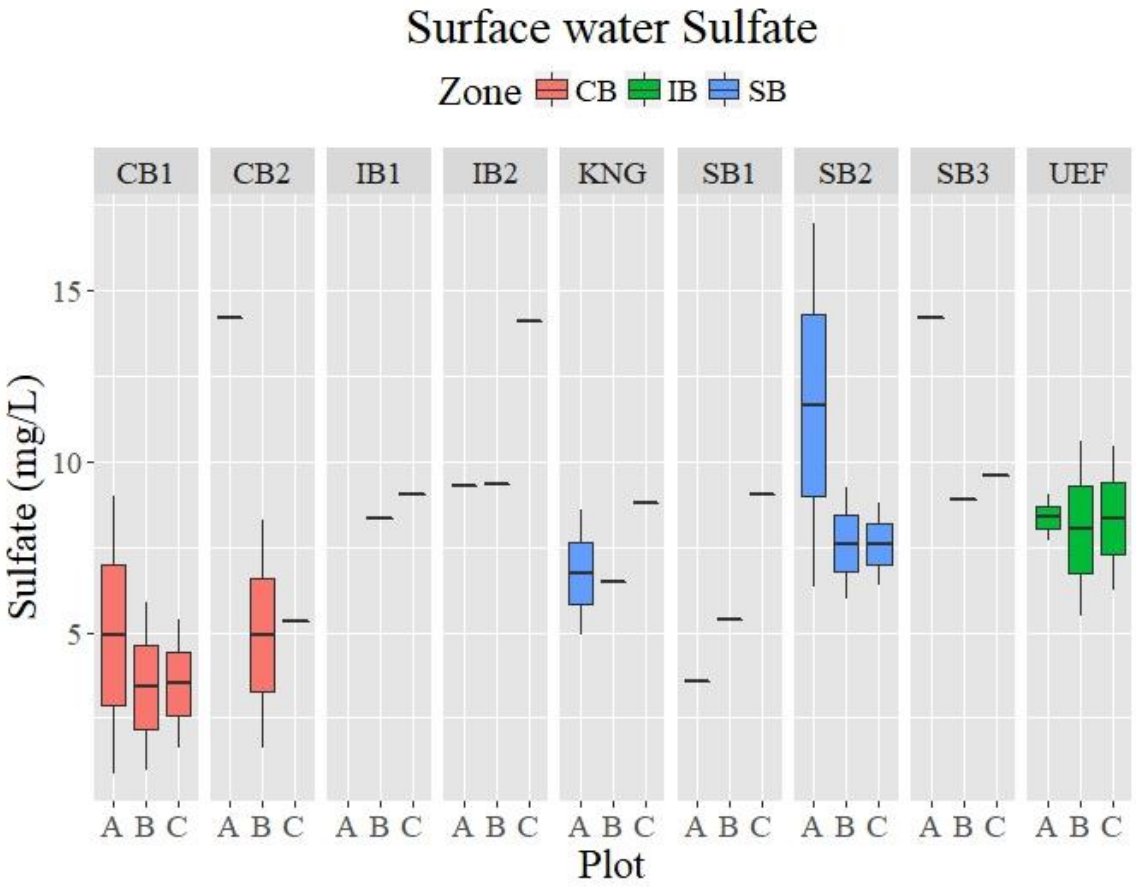

Figure S9: Surface water sulfate by individual sites (see Table S1 for more description of sites) and plot (separated within each site) and colored by habitat zone.

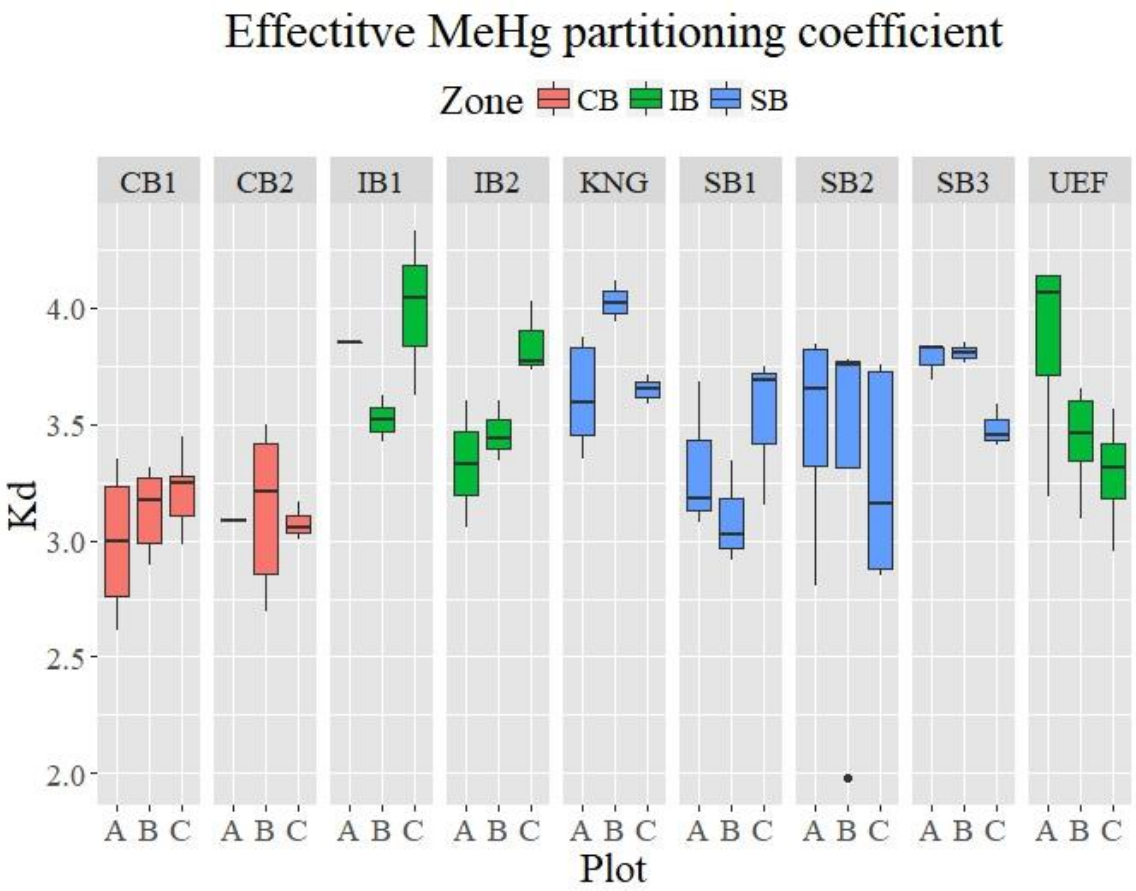

Figure S10: Effective partitioning coefficient by individual sites (see Table S1 for more description of sites) and plot (separated within each site) and colored by habitat zone.

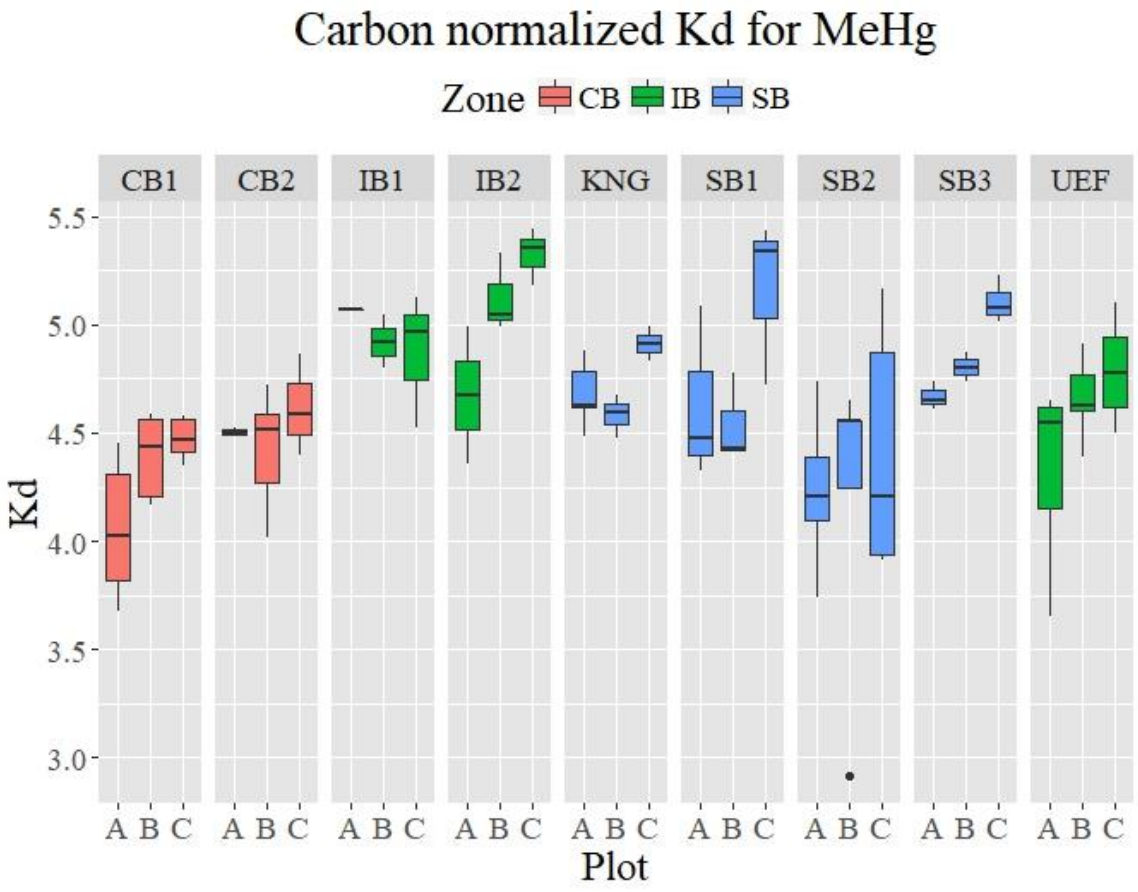

Figure S11: Carbon normalized effective partitioning coefficient for methylmercury by individual sites (see Table S1 for more description of sites) and plot (separated within each site) and colored by habitat zone.

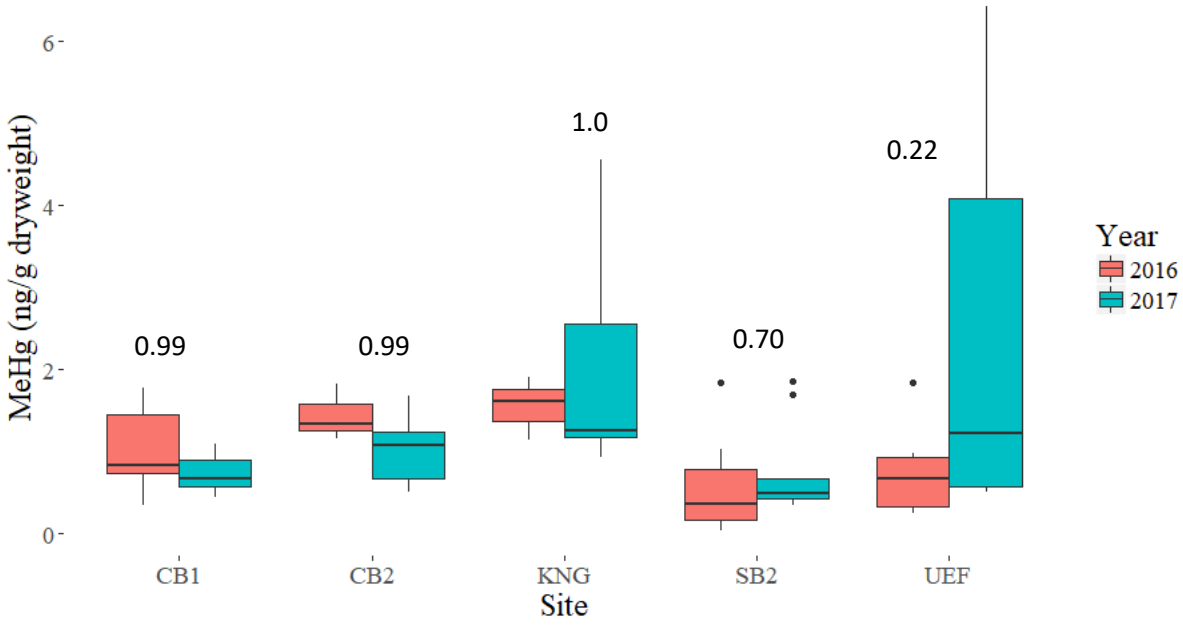

Figure S12: Comparison of sediment MeHg in 2016 and 2017. There is no significant difference between average sediment MeHg within sites in 2016 and 2017 (p-values show above bars for each site) and no consistent trend of one year appearing higher than the other. KNG and CB2 both expanded from 1 plot in 2016 to 3 plots in 2017 while CB1, SB1, and UEF had the same plots for both years. This suggests that for the variability induced by either 1) the depth differences of 0-2 cm in 2016 and 0-4 cm in 2017 or 2) climatic differences between the two years would not change the results of the ANOVA analysis if we had visited all sites in both 2016 and 2017.

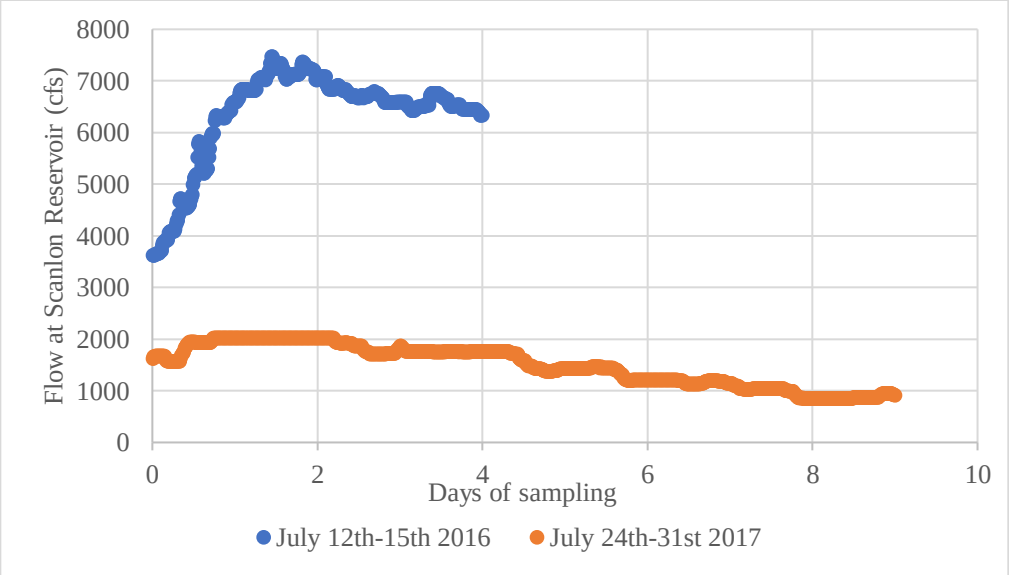

Figure S13: Comparison of St. Louis River flow during 2016 and 2017 field seasons. Flow is in cubic foot per second and time is represented as days of sampling with exact dates listed in legend.

Special section 1: Methylation rate potentials

Methods: Methylation Rates Potentials (K_{meth}): Methylation rate potentials were measured using isotope tracers in incubated core studies. Triplicate cores (4.5 cm) taken from each plot at the same time as the triplicate composite cores (described above in field methods) were injected with a mixture of stable isotope enriched $^{200}Hg^{2+}$ and $Me^{201}Hg^{+}$ Hg-Cl solution at concentrations similar to ambient IHg and MeHg. Since MeHg and IHg concentrations can vary over an order of magnitude in the SLRE and sediment composition varies between upper estuary and harbor sites, 3 different injection solutions were made: 1) low mercury/organic sediment (225 ng cm^{-3} ^{200}Hg, 6.75 ng cm^{-3} $Me^{201}Hg^{+}$), low mercury/mineral sediment (60 ng cm^{-3} ^{200}Hg, 0.75 ng cm^{-3} $Me^{201}Hg^{+}$), and high mercury/mineral sediment (450 ng cm^{-3} ^{200}Hg, 2.25 ng cm^{-3} $Me^{201}Hg^{+}$). Solution was equilibrated with filtered surface water at room temperature for 1 hour and injected through silicone covered holes in core tubes at 1 cm intervals using a 100 uL syringe. Injections started one cm above the sediment water interface and went to a depth of 9 cm below the interface. Cores were incubated at site temperature for approximately 6 hours, sectioned into 0-2 cm, 2-4 cm, and 4-8 cm sections, and were immediately frozen to stop any methylation/demethylation. Frozen samples were freeze dried and homogenized before measuring THg and MeHg isotopes.

Table S6: Summary of measured methylation rate potentials.

Zone	Site	Plot	Replicate	Year	Kmeth
CB	CB1	A	1	2016	3.21E-03
CB	CB1	A	1	2017	3.32E-03
CB	CB1	A	2	2016	4.02E-03
CB	CB1	A	2	2017	2.51E-03
CB	CB1	A	3	2016	1.66E-03
CB	CB1	A	3	2017	4.10E-03
CB	CB1	B	1	2016	1.53E-03
CB	CB1	B	1	2017	4.96E-03
CB	CB1	B	2	2016	1.49E-03
CB	CB1	B	2	2017	6.35E-03
CB	CB1	B	3	2016	2.74E-03
CB	CB1	B	3	2017	3.98E-03
CB	CB1	C	1	2016	1.25E-03
CB	CB1	C	1	2017	6.27E-03
CB	CB1	C	2	2016	6.32E-04
CB	CB1	C	2	2017	3.52E-03

CB	CB1	C	3	2016	9.86E-04
CB	CB1	C	3	2017	3.64E-03
CB	CB2	A	1	2017	3.31E-03
CB	CB2	A	2	2017	6.11E-03
CB	CB2	A	3	2017	6.99E-03
CB	CB2	B	1	2016	1.77E-03
CB	CB2	B	1	2017	2.62E-03
CB	CB2	B	2	2016	1.80E-03
CB	CB2	B	2	2017	5.76E-03
CB	CB2	B	3	2016	2.05E-03
CB	CB2	B	3	2017	5.75E-03
CB	CB2	C	1	2017	3.75E-03
CB	CB2	C	2	2017	2.99E-03
CB	CB2	C	3	2017	4.88E-03
IB	IB1	A	1	2017	2.20E-03
IB	IB1	A	2	2017	3.53E-03
IB	IB1	A	3	2017	2.42E-03
IB	IB1	B	1	2017	1.15E-03
IB	IB1	B	2	2017	2.45E-03
IB	IB1	B	3	2017	1.90E-03
IB	IB1	C	1	2017	1.53E-03
IB	IB1	C	2	2017	9.71E-04
IB	IB1	C	3	2017	1.61E-03
IB	IB2	A	1	2017	2.60E-03
IB	IB2	A	2	2017	1.18E-03
IB	IB2	A	3	2017	1.58E-03
IB	IB2	B	1	2017	1.11E-03
IB	IB2	B	2	2017	2.18E-03
IB	IB2	B	3	2017	3.41E-03
IB	IB2	C	1	2017	3.84E-03
IB	IB2	C	2	2017	1.21E-03
IB	IB2	C	3	2017	6.41E-03
IB	IB3	B	1	2017	5.55E-03
IB	IB3	B	2	2017	2.26E-03
IB	IB3	B	3	2017	1.08E-03
IB	LEF	B	1	2017	7.67E-03
IB	LEF	B	2	2017	1.05E-02
IB	LEF	B	3	2017	4.06E-03
IB	UEF	A	1	2016	4.77E-04
IB	UEF	A	1	2017	6.54E-03
IB	UEF	A	2	2016	3.89E-04
IB	UEF	A	2	2017	1.23E-02
IB	UEF	A	3	2016	

IB	UEF	A	3	2017	1.91E-03
IB	UEF	B	1	2016	6.30E-04
IB	UEF	B	1	2017	3.07E-03
IB	UEF	B	2	2016	5.68E-04
IB	UEF	B	2	2017	7.59E-03
IB	UEF	B	3	2016	1.36E-03
IB	UEF	B	3	2017	
IB	UEF	C	1	2016	9.08E-04
IB	UEF	C	1	2017	
IB	UEF	C	2	2016	1.20E-03
IB	UEF	C	2	2017	
IB	UEF	C	3	2016	7.60E-04
IB	UEF	C	3	2017	
SB	KNG	A	1	2016	1.13E-03
SB	KNG	A	1	2017	
SB	KNG	A	2	2016	9.17E-04
SB	KNG	A	2	2017	5.46E-03
SB	KNG	A	3	2016	4.31E-03
SB	KNG	A	3	2017	6.04E-03
SB	KNG	B	1	2017	5.40E-03
SB	KNG	B	2	2017	3.27E-03
SB	KNG	B	3	2017	6.94E-03
SB	KNG	C	1	2017	4.80E-04
SB	KNG	C	2	2017	3.25E-03
SB	KNG	C	3	2017	3.65E-03
SB	SB1	A	1	2016	3.45E-03
SB	SB1	A	2	2016	3.38E-03
SB	SB1	A	3	2016	3.32E-03
SB	SB1	B	1	2016	1.41E-03
SB	SB1	B	2	2016	1.64E-03
SB	SB1	B	3	2016	2.51E-03
SB	SB1	C	1	2016	1.49E-03
SB	SB1	C	2	2016	1.39E-03
SB	SB1	C	3	2016	1.69E-03
SB	SB2	A	1	2016	1.20E-03
SB	SB2	A	1	2017	7.86E-03
SB	SB2	A	2	2016	1.51E-03
SB	SB2	A	2	2017	5.01E-03
SB	SB2	A	3	2016	
SB	SB2	A	3	2017	3.91E-03
SB	SB2	B	1	2016	1.69E-03
SB	SB2	B	1	2017	5.14E-03
SB	SB2	B	2	2016	7.94E-03

SB	SB2	B	2	2017	6.40E-03
SB	SB2	B	3	2016	9.73E-03
SB	SB2	B	3	2017	1.60E-02
SB	SB2	C	1	2016	1.29E-03
SB	SB2	C	1	2017	2.43E-02
SB	SB2	C	2	2016	5.27E-03
SB	SB2	C	2	2017	1.53E-02
SB	SB2	C	3	2016	1.86E-03
SB	SB2	C	3	2017	1.08E-02
SB	SB3	A	1	2017	3.65E-03
SB	SB3	A	2	2017	
SB	SB3	A	3	2017	
SB	SB3	B	1	2017	
SB	SB3	B	2	2017	
SB	SB3	B	3	2017	
SB	SB3	C	1	2017	
SB	SB3	C	2	2017	2.71E-03
SB	SB3	C	3	2017	1.04E-02

Special section 2: Lab flux study

Methods: *Ex-situ* diffusive flux studies were conducted using undisturbed sediment cores (6.35 cm diameter) subject to a 24-hour laboratory incubation. This time was selected based on previous studies (Beck et al. 2014). Five replicate sediment cores were collected using a gravity core, capped, and sealed with electrical tape to be brought back to the lab. The overlying water was carefully replaced with 500 mL filtered river water. Initial surface water samples were collected in by hand from the newly replaced water in the core tube directly above the sediment using trace-metal clean methods and new PETG bottles. Surface water in the flux studies was analyzed for filtered total- and methyl- mercury. A small stream of filtered air was used to mix the overlying water to keep the water column oxidized and minimize the buildup of MeHg directly above the sediment water interface. Surface water samples were taken at 0, 12, and 24 hrs.

Table S7: Results from lab flux study, dissolved MeHg concentrations in ng L^{-1}. Data for each replicate and average and standard deviation of each replicate are provided in the table.

Site and replicate	0	12	24	48	60	anoxic
CB1 1	0.030	0.144	0.155	0.195	0.224	0.277
CB1 2	0.139	0.108	0.139	0.163	0.227	0.157
CB1 3	0.115	0.323	0.311	0.243	0.349	
CB1 4	0.100	0.137	0.115	0.130	0.154	0.163
CB1 5	0.057	0.071	0.117	0.162	0.198	
CB1 average	0.088	0.156	0.167	0.178	0.230	0.199
CB2 SD	0.039	0.087	0.073	0.038	0.065	0.055
IB1 1	0.151	0.158	0.148	0.158	0.160	0.135
IB1 2	0.152	0.148	0.162	0.165	0.159	0.080
IB1 4	0.129	0.149	0.098	0.135	0.184	0.149
IB1 5	0.199	0.155	0.144			
IB1 Average	0.158	0.153	0.138	0.152	0.168	0.121
IB1 SD	0.026	0.004	0.024	0.012	0.012	0.030
IB2 1	0.137	0.118	0.113	0.120	0.112	0.169
IB2 2	0.137	0.107	0.102	0.103	0.118	0.128
IB2 3	0.138	0.125	0.020	0.115	0.225	0.125
IB2 4	0.145	0.121	0.098	0.119	0.126	0.095
IB2 5	0.149	0.114	0.143	0.142	0.141	0.156
IB2 Average	0.141	0.117	0.095	0.120	0.145	0.135
IB2 SD	0.005	0.006	0.041	0.012	0.042	0.026
UEF 1	0.158	0.179	0.129	0.214	0.177	0.041
UEF 2	0.030	0.168	0.169	0.108	0.170	0.140
UEF 3	0.172	0.136	0.172	0.378	0.171	

UEF 4	0.078	0.145	0.257	0.248	0.175	0.681
UEF 5	0.014	0.114	0.114	0.201	0.170	0.146
UEF Average	0.090	0.148	0.168	0.230	0.173	0.252
UEF SD	0.065	0.023	0.050	0.087	0.003	0.251
SB3 1	0.159	0.276	0.690	0.548	0.442	1.490
SB3 2	0.131	0.436	0.656	0.842	0.683	0.871
SB3 3	0.092	0.084	0.165	0.087	0.090	0.350
SB3 4	0.140	0.267	0.297	0.433	0.224	0.591
SB3 5	0.179	0.271	0.365	0.654	0.458	0.710
SB3 Average	0.140	0.267	0.435	0.513	0.379	0.802
SB3 SD	0.029	0.112	0.205	0.252	0.205	0.384
KNG 1	0.174	0.092	0.030	0.097	0.103	0.643
KNG 2	0.174	0.058	0.003	0.084	0.083	0.086
KNG 3	0.174	0.077	0.112	0.105	0.046	0.227
KNG 4	0.174	0.163	0.101	0.111	0.121	0.142
KNG 5	0.174	0.039	0.107	0.137	0.103	0.074
KNG Average	0.174	0.086	0.070	0.107	0.091	0.234
KNG SD	0.000	0.043	0.045	0.018	0.026	0.211

Special section 3: Application: a proposed conceptual model describing Hg cycling in different aquatic ecosystems

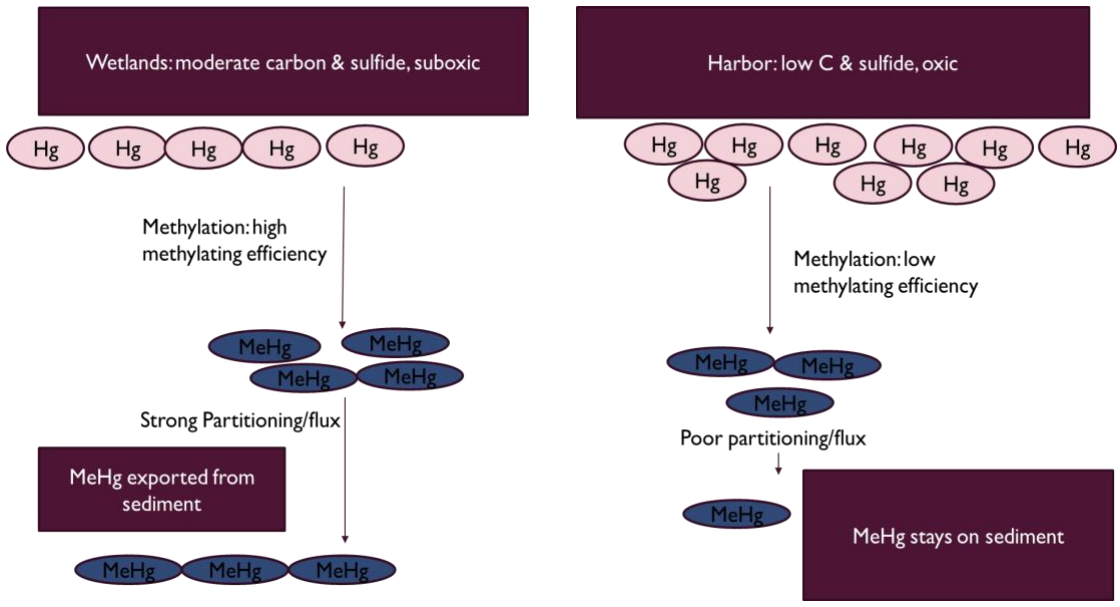

To synthesize the results and discussion above in a coherent and applicable manner, a conceptual model for understanding MeHg production and transport in aquatic environments is described here. The proposed conceptual model attempts to provide context for the processes of MeHg production, partitioning, and flux in the sediment of a complex freshwater aquatic system with historical industrial influence. The actual point of entry into the food web depends on food web structure, but this conceptual model can be used to understand whether MeHg tends to stay on the sediment solid phase or be transported to surface waters. These two simplified scenarios (or others defined for relevant ecosystem comparisons) could inform models for bioaccumulation if the food web structure is known.

For simplicity, the conceptual model is split into two sections, one representative of the wetland-like sheltered bay or clay bay habitat zones and the other representative of the low carbon environments with mostly oxic surface waters of the industrial bay habitat zone. The conceptual model begins with the production of MeHg from available inorganic Hg in the sediments. Areas like the SLRE wetlands that are efficient producers of MeHg will see a greater proportion of the available inorganic Hg methylated, which is represented by the change in color of the "Hg" bubbles from pink to blue. In the presence of moderate

porewater sulfide (5-15 μmol L^{-1}) and moderate solid phase carbon (4-7% carbon), the MeHg is more likely to move into the porewater and potentially set up a diffusive flux gradient towards surface water. MeHg that stays in sediment could continually be methylated and demethylated in the same location and not make it to surface waters.

The introduction of Hg to waters via atmospheric deposition means that most open water systems will continue to have an input source of Hg for long into the future. Limiting the production of MeHg by stopping atmospheric deposition is challenging. However, using ecologically-delineated areas as a basis for evaluating Hg cycling could have utility in modeling or remedy selection. A framework for characterizing where and how MeHg moves can be useful for resource managers attempting to remediate or restore habitats that could already be experiencing mercury problems (such as the SLRE) or to guide the creation of a TMDL by comparing internal versus external loads. If a resource manager knows that the base of the food web is tied to the sediment or porewaters they can use this model to address the conditions that promote retention of MeHg in sediment or porewaters or anticipate changes resulting from other management actions. Alternatively, if the food web is more closely tied to the water column, understanding which sediments might be prone to establishing concentration gradients that support diffusive transport could also be helpful. This can be accomplished by measure MeHg or Hg in the porewater and surface water. The implications of surface water MeHg vs. porewater MeHg on bioaccumulation should utilize in-situ measures of MeHg concentration at the base of the food web. While this paper did not directly examine food web structure or biota Hg trends, a second component of this study investigated food web structure and MeHg accumulation in the SLRE, and the results of this paper will be useful for determining the relationship of sediment, porewater, and surface water MeHg to biota Hg.

This conceptual model was constructed using solid phase %MeHg to determine how efficient the methylating community was. Log K_d was calculated using sediment and porewater MeHg concentrations but measuring porewater sulfide and sediment carbon can provide insight as to whether MeHg is more likely to bind to the solid phase or migrate to porewaters. Porewater and surface water MeHg concentrations can be used to estimate the potential diffusive flux gradient and how likely an area of sediments is to load MeHg into the overlying surface water and connected aquatic system. We used this method in our study and found a sustained diffusive flux gradient was observed during both high and low flow conditions. However, a large

overall mass of MeHg is still transported to the SLRE from the wetland-rich watershed. The extent to which internal sources of MeHg contribute to MeHg in food web of the SLRE needs to be further investigated, with a focus on the the diverse hydrologic and geochemical conditions present in different portions of the estuary.

The conceptual model presented here provides the basis for how mercury can move through the diverse habitats presents in a freshwater environment and highlight some of the most important geochemical factors that appear to influence MeHg production, partitioning, and diffusive flux from sediment.